Science Immunology
AAAS

immunology.sciencemag.org/cgi/content/full/4/34/eaav6778/DC1

Supplementary Materials for

AIRE expression controls the peripheral selection of autoreactive B cells

Joel Sng, Burcu Ayoglu, Jeff W. Chen, Jean-Nicolas Schickel, Elise M. N. Ferre, Salomé Glauzy, Neil Romberg, Manfred Hoenig, Charlotte Cunningham-Rundles, Paul J. Utz, Michail S. Lionakis, Eric Meffre*

*Corresponding author. Email: eric.meffre@yale.edu

Published 12 April 2019, *Sci. Immunol.* **4**, eaav6778 (2019)
DOI: 10.1126/sciimmunol.aav6778

The PDF file includes:

Other Supplementary Material for this manuscript includes the following:

(available at immunology.sciencemag.org/cgi/content/full/4/34/eaav6778/DC1)

Supplementary Figures

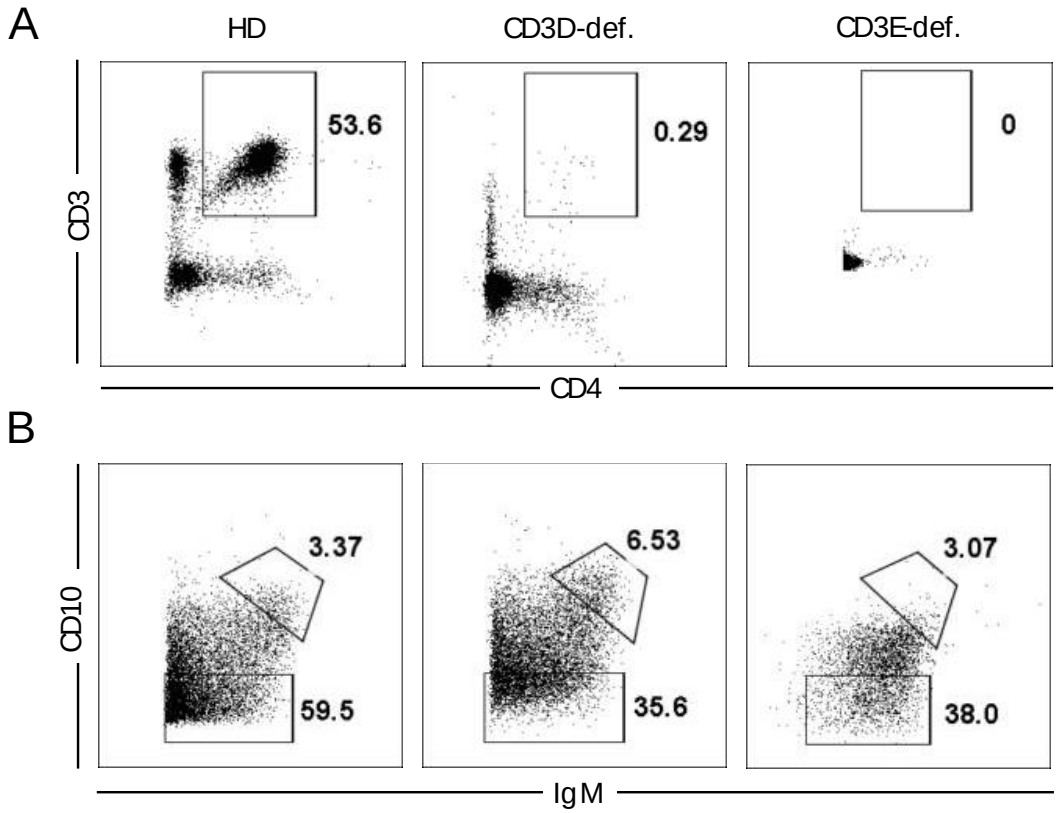

Fig. S1, related to Fig. 1. CD3D- and CD3E-deficient patients lack circulating $CD3^{+}CD4^{+}$ T cells. (A) Representative CD3 and CD4 staining on total lymphocytes from a healthy donor (HD), a CD3D-deficient (CD3D-def.), and a CD3E-deficient (CD3E-def.) patient. (B) Representative CD10 and IgM staining on gated $CD19^{+}CD27^{-}$ naïve B cells in a HD, a CD3D-def., and a CD3E-def. patient. Gating strategy for new emigrant/transitional ($CD10^{hi}IgM^{hi}$) and mature naïve ($CD10^{-}IgM^{+}$) subsets are shown.

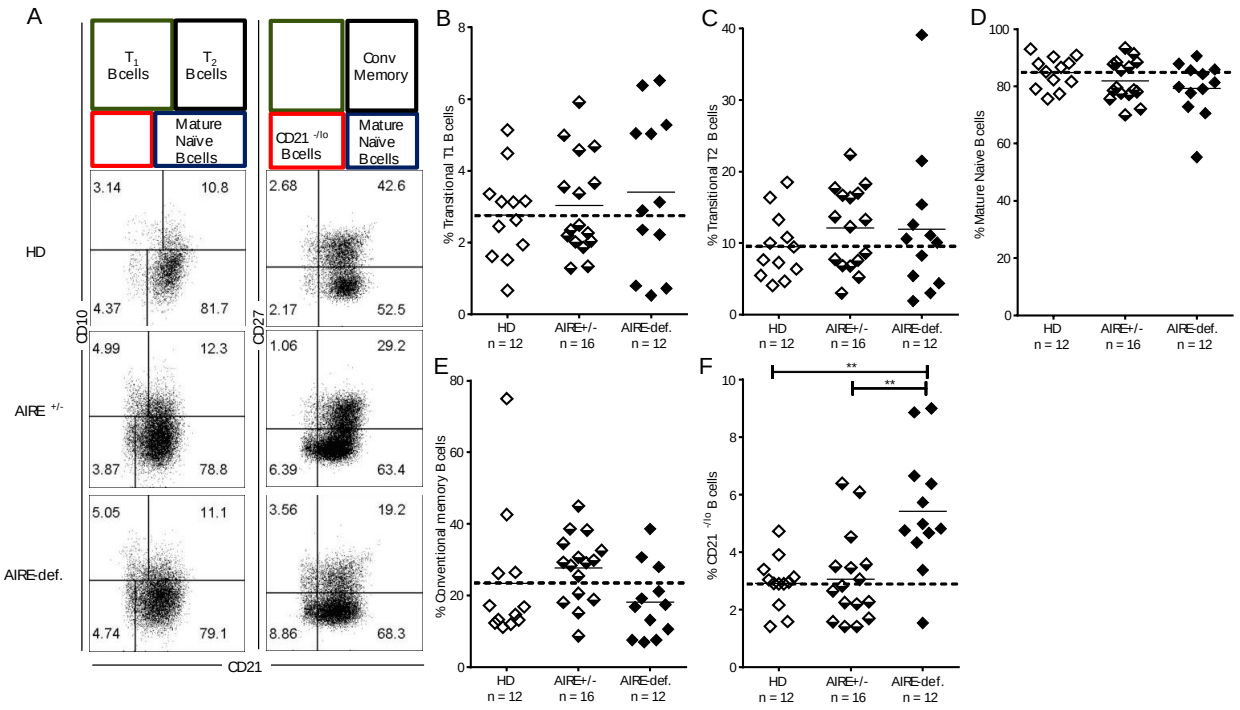

Fig. S2, related to Fig. 1. AIRE-deficient patients display elevated frequencies of $CD19^{+}CD27^{-}CD10^{-}CD21^{-/lo}$ B cells. (A) Representative CD21 and CD10 staining (left) on $CD19^{+}CD27^{-}$ B cells and CD21 and CD27 staining (right) on $CD19^{+}$ B cells from a healthy donor (HD), AIRE+/- subject and AIRE-deficient patient. Summarized frequencies of (B) $CD19^{+}CD27^{-}CD10^{high}CD21^{-/lo}$ transitional T1, (C) $CD19^{+}CD27^{-}CD10^{+}CD21^{+}$ transitional T2, (D) $CD19^{+}CD27^{-}CD10^{-}CD21^{+}$ mature naïve, (E) $CD19^{+}CD27^{+}CD10^{-}CD21^{+}$ conventional memory, and (F) $CD19^{+}CD27^{-}CD10^{-}CD21^{-/lo}$ B cells are represented. Each symbol represents an individual, solid lines show the mean and dashed line indicates the averaged mean value for HDs. Statistically significant differences are indicated.

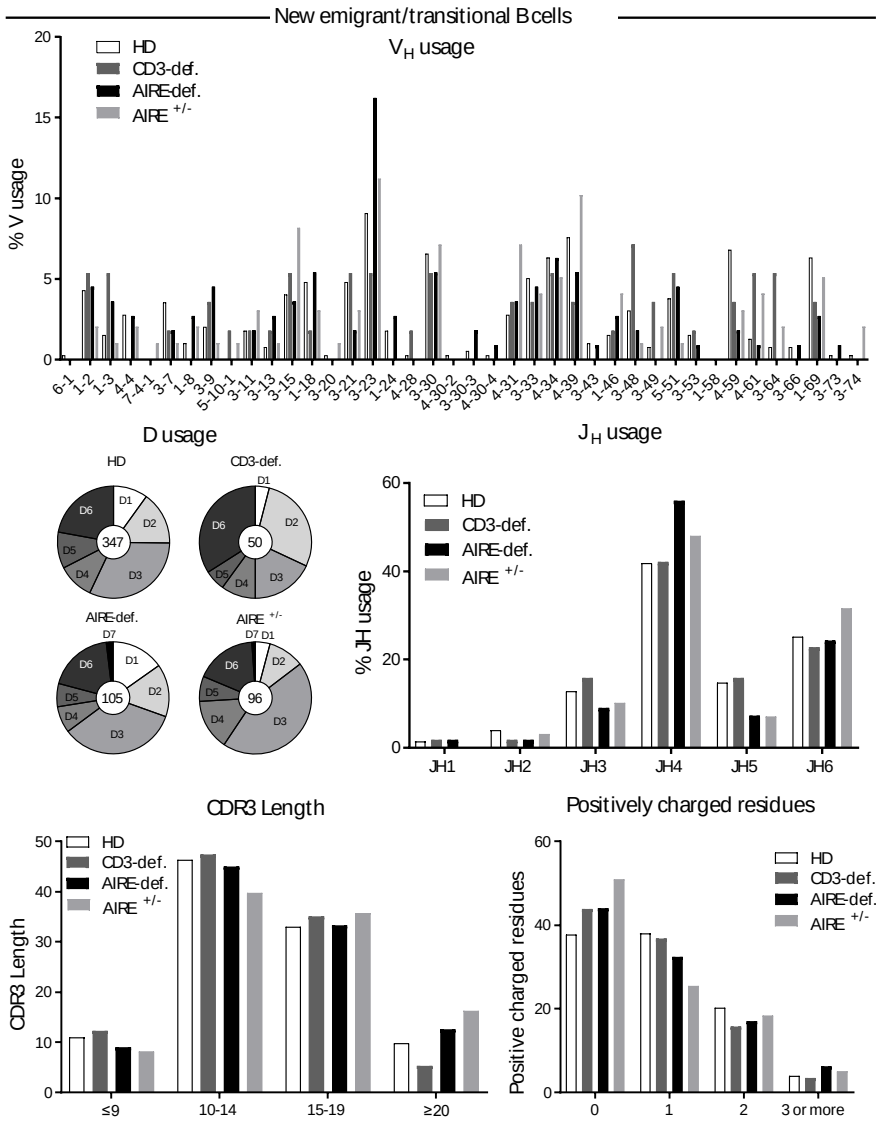

Fig. S3, related to Fig. 1. Immunoglobulin heavy chain gene usage in new emigrant/transitional B cells from CD3- and AIRE-deficient patients and AIRE$^{+/-}$ heterozygous individuals. V_H, D and J_H gene segment usage, third complementarity-determining region (CDR3) length, and positively charged amino acid content are compared between new emigrant/transitional B cells from 13 healthy controls (HDs), two CD3-deficient (CD3-def.) patients, four AIRE-deficient (AIRE-def.) patients, and three AIRE heterozygous (AIRE$^{+/-}$) subjects.

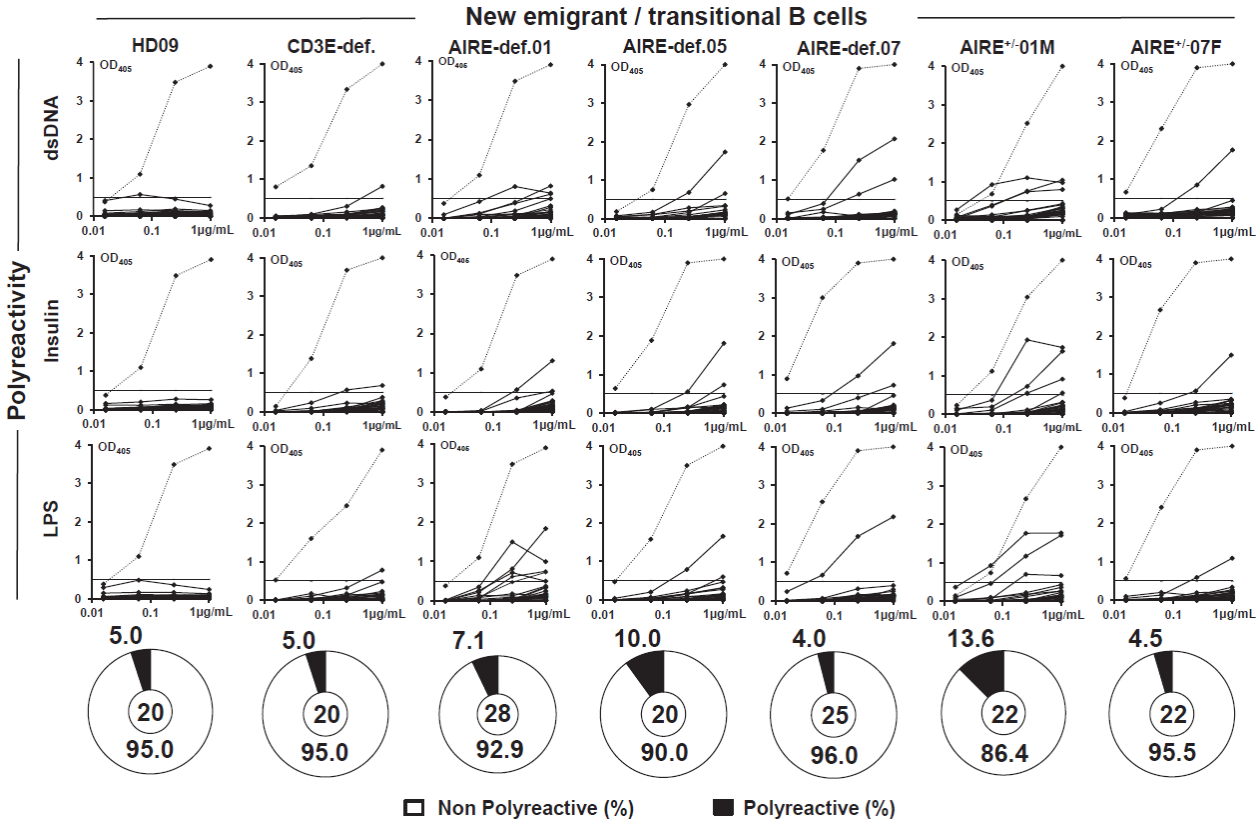

Fig. S4, related to Fig. 1. Low frequencies of polyreactive new emigrant/transitional B cells in CD3- and AIRE-deficient patients and AIRE$^{+/-}$ heterozygous individuals. Recombinant antibodies expressed by CD19^{+}CD27^{-}CD21$^{-/lo}$CD10^{+}IgM^{hi} new emigrant/transitional B cells from a representative healthy donor (HD), a CD3E-deficient (CD3E-def.) patient, three AIRE-deficient patients (AIRE-def.) and two AIRE$^{+/-}$ heterozygous relatives (AIRE$^{+/-}$) were tested by ELISA for polyreactivity against dsDNA, insulin, and LPS. Solid lines show binding for each cloned recombinant antibody. Dotted lines show ED38-positive control. Horizontal lines show cutoff OD_{405} for positive reactivity. Antibodies were considered polyreactive when they recognized all three antigens. For each individual, the frequency of polyreactive B cells are summarized in pie charts, with the number of antibodies tested shown in the center. Please also see Figure 1.

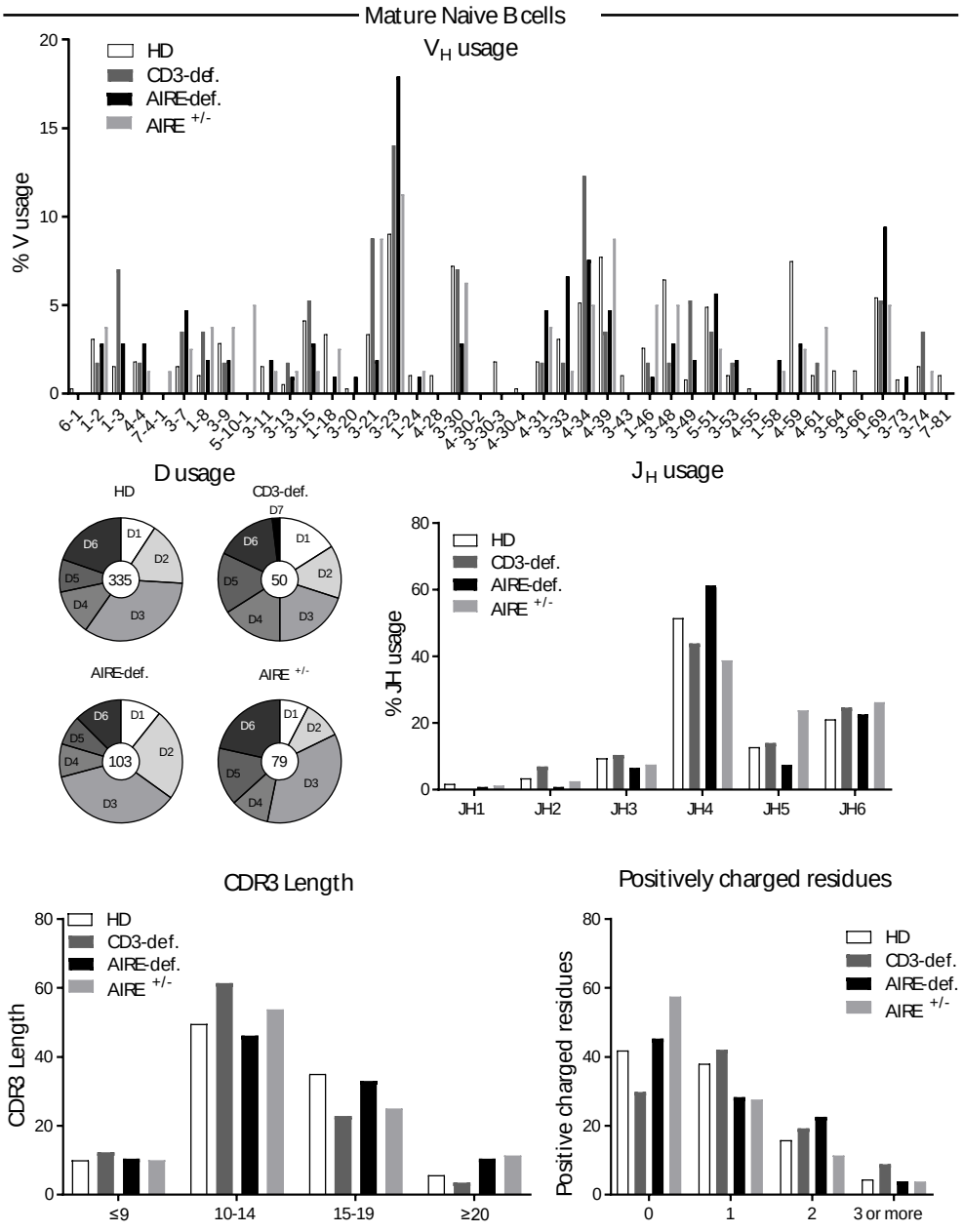

Fig. S5, related to Fig. 2. Immunoglobulin heavy chain gene usage in mature naïve B cells from CD3- and AIRE-deficient patients and AIRE$^{+/-}$ heterozygous individuals. V_H, D and J_H gene segment usage, third complementarity-determining region (CDR3) length, and positively charged amino acid content are compared between mature naive B cells from 13 healthy controls (HDs), two CD3-deficient patients (CD3-def.), four AIRE-deficient patients (AIRE-def.) and three AIRE$^{+/-}$ heterozygous subjects (AIRE$^{+/-}$).

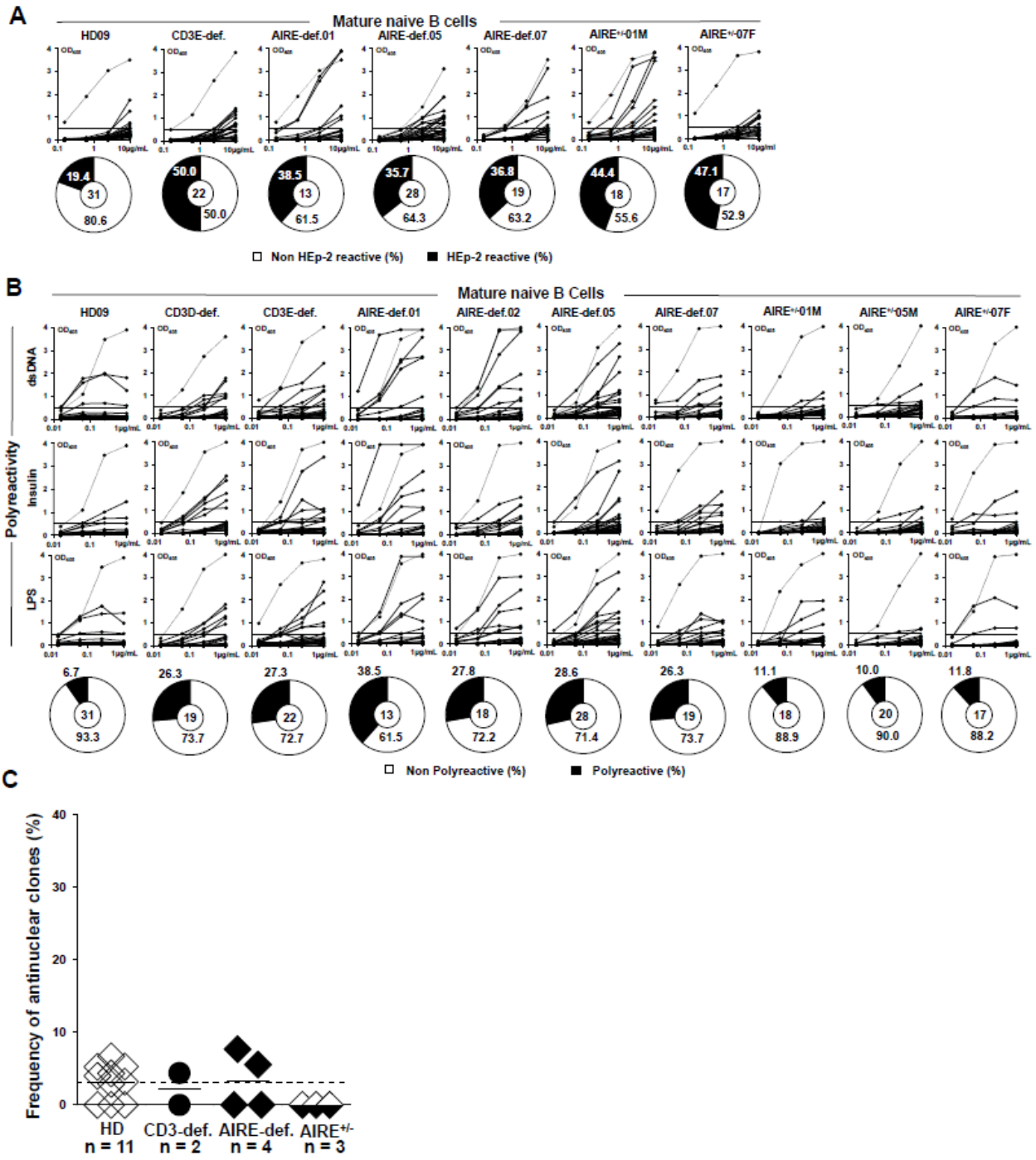

Fig. S6, related to Fig. 2. Defective peripheral B cell tolerance checkpoint in CD3- and AIRE-deficient patients. Recombinant antibodies expressed by $CD19^{+}CD21^{+}CD10^{-}IgM^{+}CD27^{-}$ mature naive B cells from a representative healthy donor (HD), a CD3E-deficient patient (CD3E-def.), three AIRE-deficient patients (AIRE-def.) and two AIRE heterozygous relatives ($AIRE^{+/-}$)

were tested by ELISA for (A) HEp-2 reactivity, (B) polyreactivity against dsDNA, insulin, and LPS, and. Solid lines show binding for each cloned recombinant antibody. Dotted lines show ED38-positive control. Horizontal lines show cutoff OD_{405} for positive reactivity. For each individual, the frequency of HEp-2 B cells are summarized in pie charts, with the number of antibodies tested shown in the center. (C) Anti-nuclear mature naïve B cell frequencies from HDs, CD3-deficient patients, AIRE-deficient patients, and AIRE heterozygous subjects. Each symbol represents an individual, solid lines show the mean and dashed line indicates the averaged mean value for HDs. Please also see Figure 2.

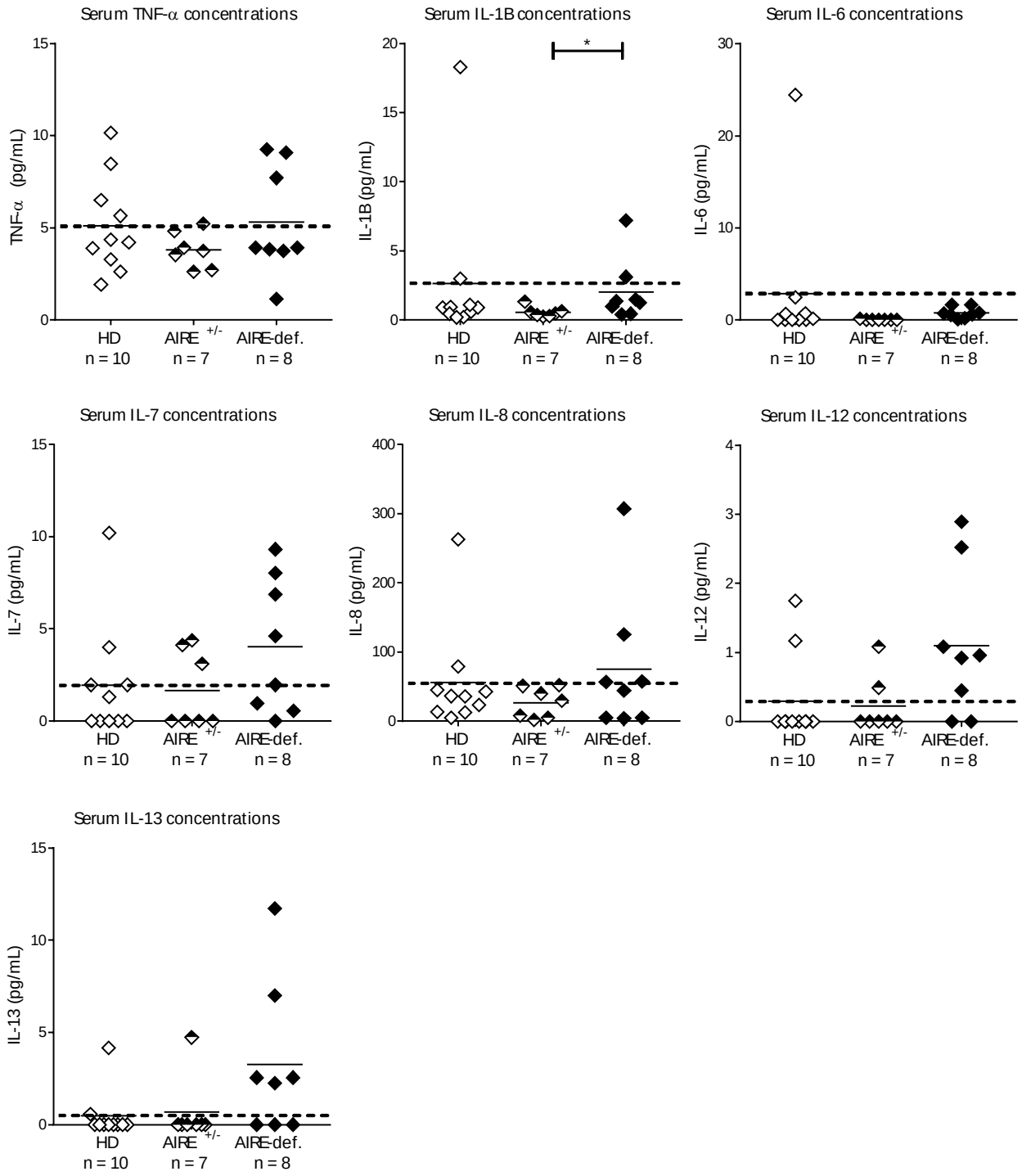

Fig. S7, related to Fig. 3. Serum cytokine concentrations in HDs, AIRE$^{+/-}$ carriers, and AIRE-deficient patients measured by Luminex. Each symbol represents an individual, solid lines show the mean and dashed line indicates the averaged mean value for HDs. Statistically significant differences are indicated.

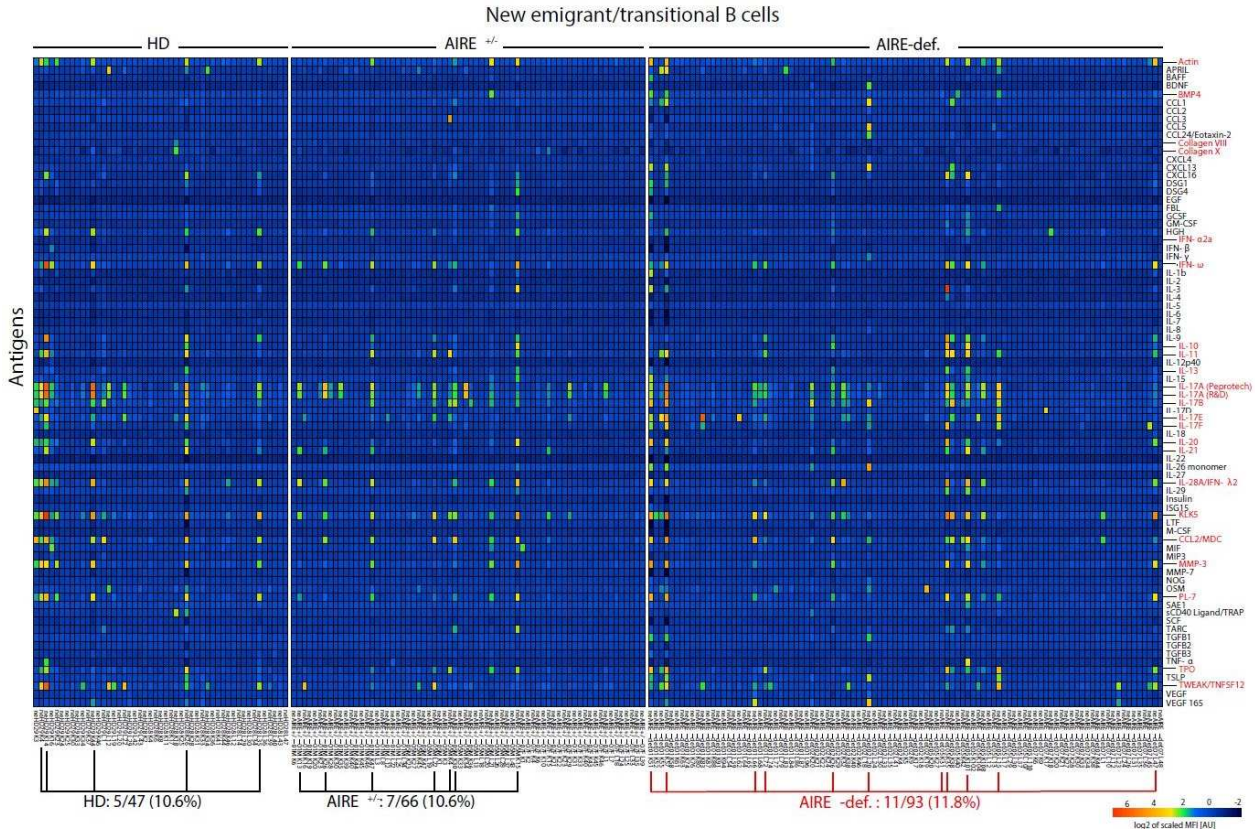

Fig. S8, related to Fig. 4. Autoantigen array analysis of recombinant antibodies cloned from single-cell sorted new emigrant/transitional B cells from HDs, AIRE$^{+/-}$ heterozygous relatives, and AIRE-deficient patients. Heatmap displaying reactivity of individual new emigrant/transitional B cells from healthy donors (HD, n=2), AIRE$^{+/-}$ heterozygous subjects (AIRE$^{+/-}$, n=3) and AIRE-deficient patients (AIRE-def. n=4) against selected cytokines and other self-antigens. The frequencies of self-reactive new emigrant/transitional B cells are similar in HDs, AIRE$^{+/-}$ subjects, and AIRE-deficient patients.

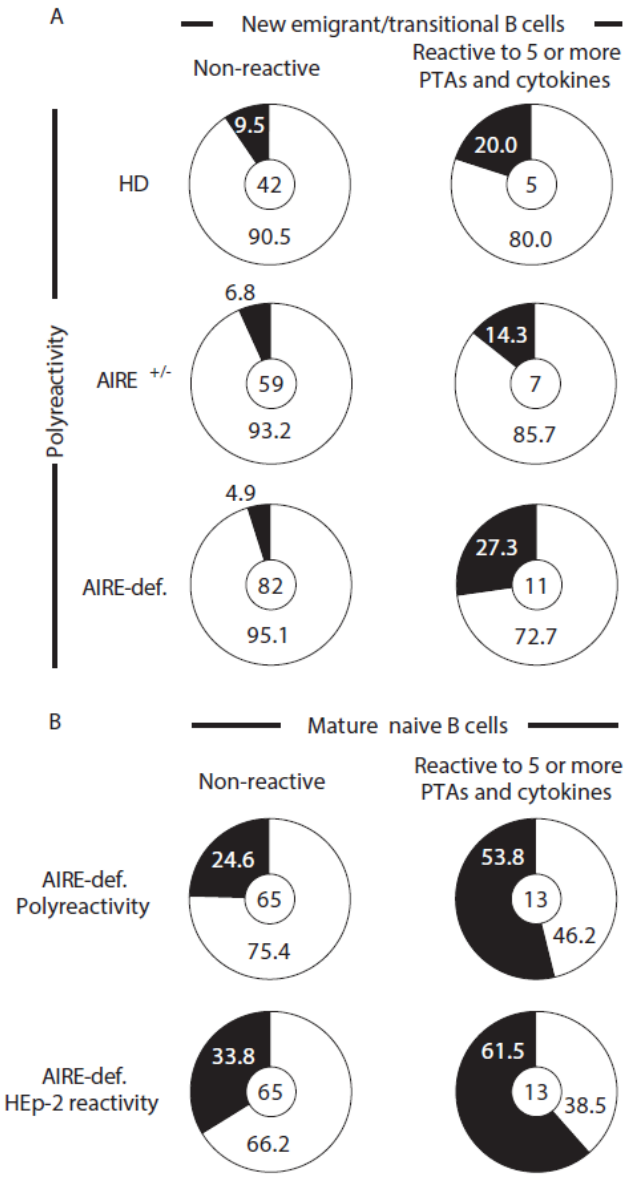

Fig. S9, related to Fig. 4. Autoreactive clones identified in autoantigen array were previously identified as polyreactive and/or HEp-2 reactive by ELISAs. Recombinant antibodies expressed by (A) new emigrant/transitional and (B) mature naive B cells from pooled healthy donors (HD, n=2), AIRE$^{+/-}$ heterozygous subjects (AIRE$^{+/-}$, n=3) and AIRE-deficient patients (AIRE-def., n=4) that are non-reactive (left) or reactive (right) to five or more peripheral tissue antigens and cytokines are enriched in clones previously characterized as polyreactive and/or HEp-2 reactive by ELISA. Data are summarized in pie charts with the number of antibodies analyzed shown in the center.

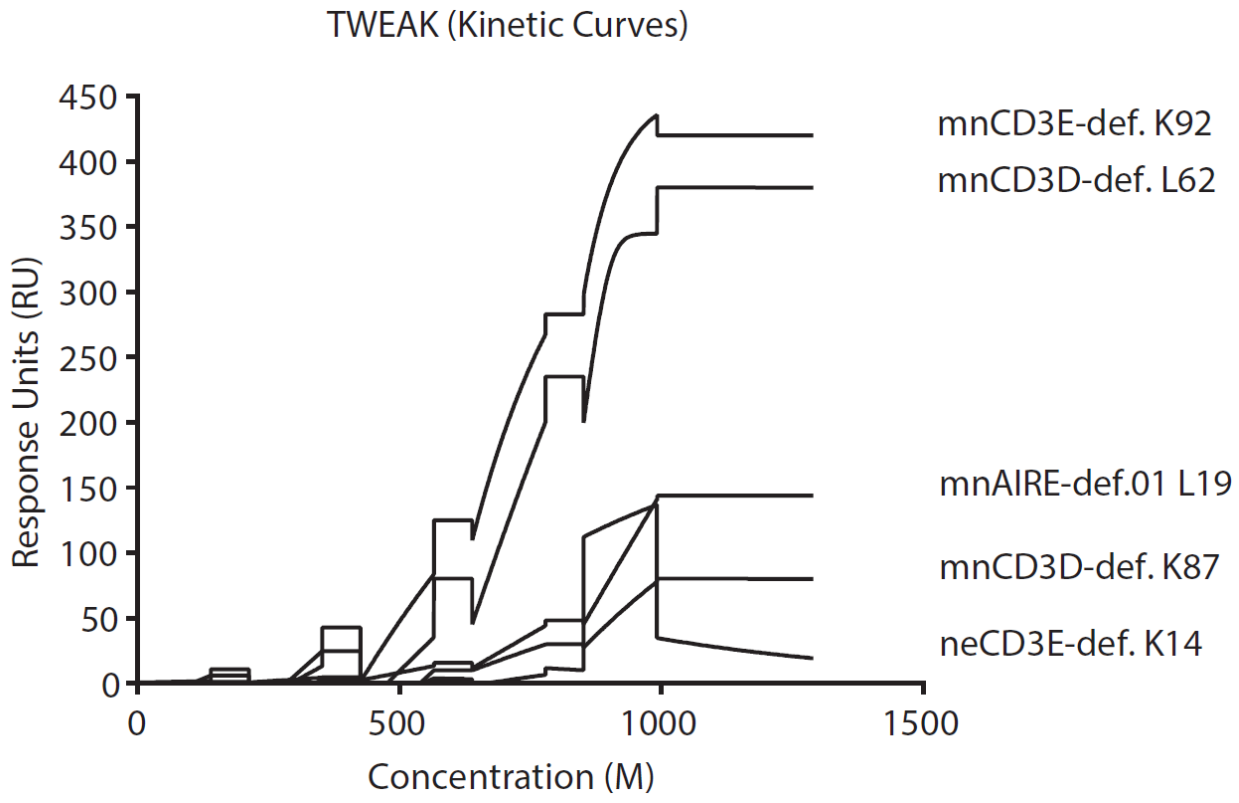

Fig. S10, related to Fig. 5. TWEAK kinetic binding curves of antibodies from new emigrant/transitional and mature naïve B cells from CD3- and AIRE-deficient patients. Surface plasmon resonance analysis of high affinity (10μM to < 1 nM range) antibody binding to the AIRE-independent antigen TWEAK.

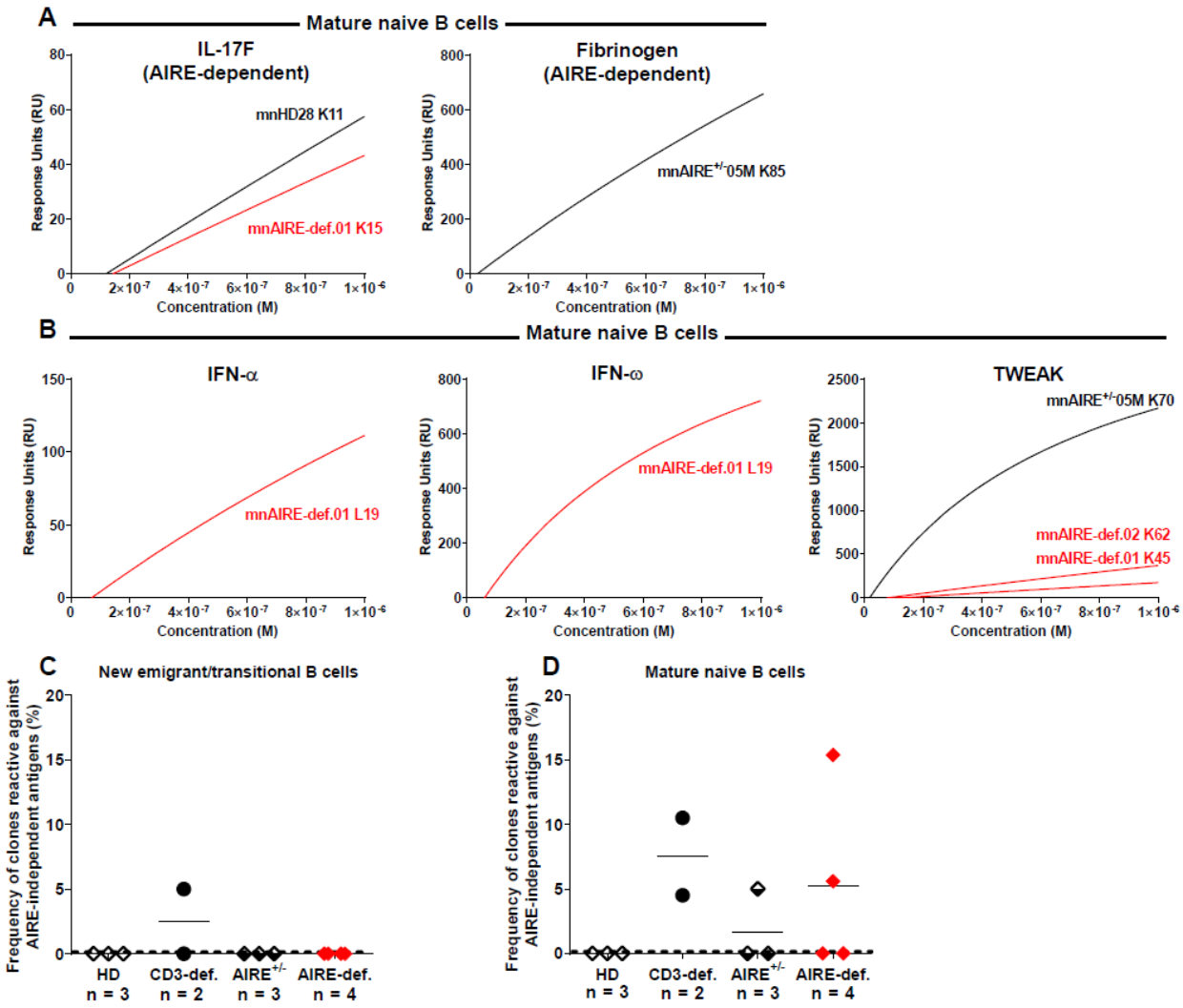

Fig. S11, related to Fig. 5. Increase frequencies of AIRE-independent antigen-reactive clones in the mature naïve B cell compartment of CD3- and AIRE-deficient patients. Surface plasmon resonance analysis of antibody binding to the AIRE-dependent antigens, IL-17F and Fibrinogen (A) and AIRE-independent antigens, IFN-α and IFN-ω and TWEAK (B) by recombinant antibodies cloned from single mature naïve B cells from three healthy donors (HDs), CD3-def. patients (CD3-def.), AIRE heterozygous ($AIRE^{+/-}$) subjects, and AIRE-deficient (AIRE-def.) patients. Frequencies of (C) new emigrant/transitional and (D) mature naïve B cells from HDs, CD3-def. patients, $AIRE^{+/-}$ subjects, and AIRE-def. patients reactive against AIRE-independent antigens.

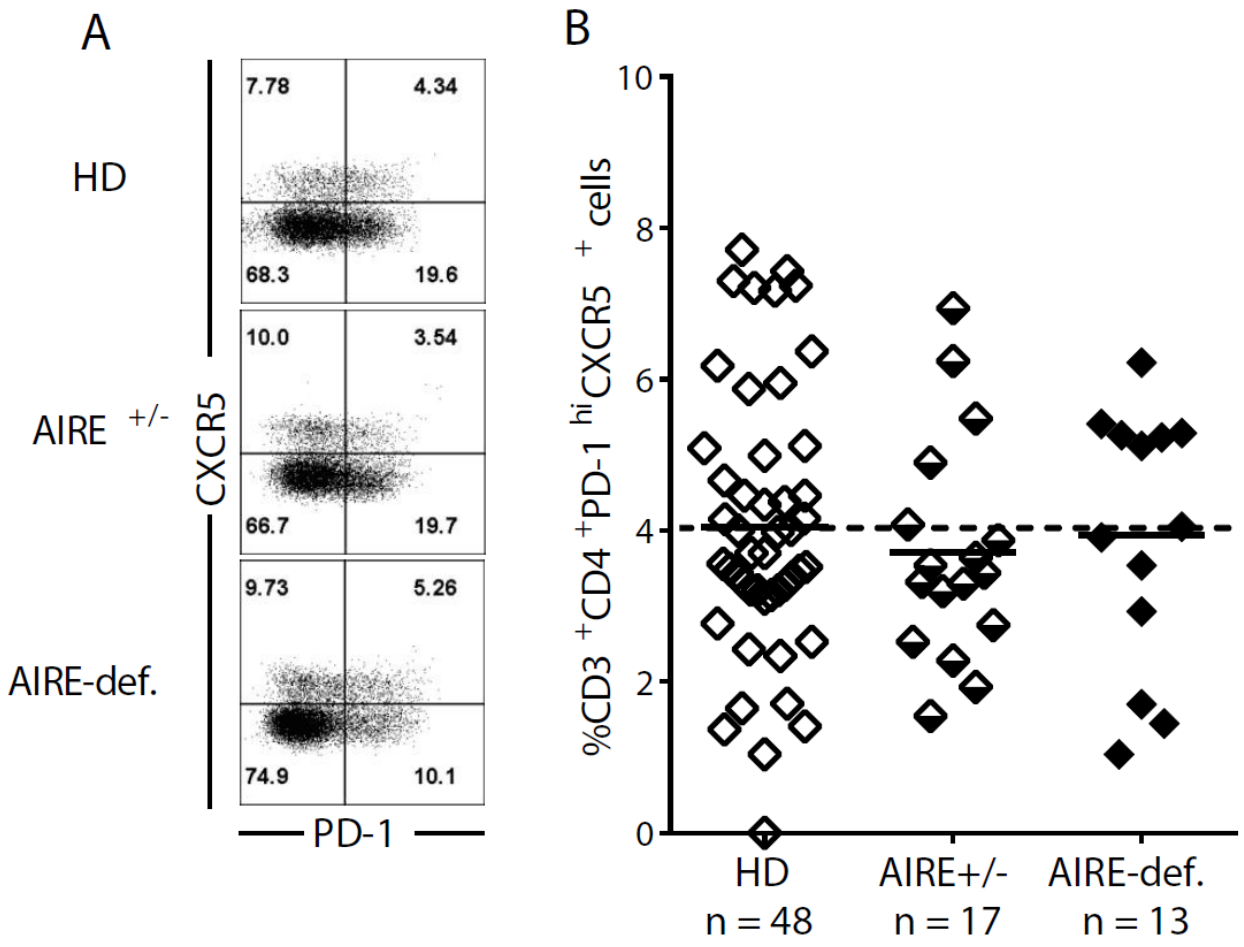

Fig. S12, related to Fig. 6. Similar frequencies of T_{FH} cells in HDs, AIRE$^{+/-}$ heterozygous individuals, and AIRE-deficient patients. (A) Representative PD-1 and CXCR5 staining on CD3^{+}CD4^{+} cells from a healthy donor (HD), AIRE$^{+/-}$ heterozygous (AIRE$^{+/-}$) subject, and AIRE-deficient (AIRE-def.) patient. (B) CD3^{+}CD4^{+}PD-1^{hi}CXCR5^{+} Tfh cell frequencies in HDs, AIRE+/- subjects, and AIRE-def. patients. Each symbol represents an individual, solid lines show the mean and dashed line indicates the averaged mean value for HDs.

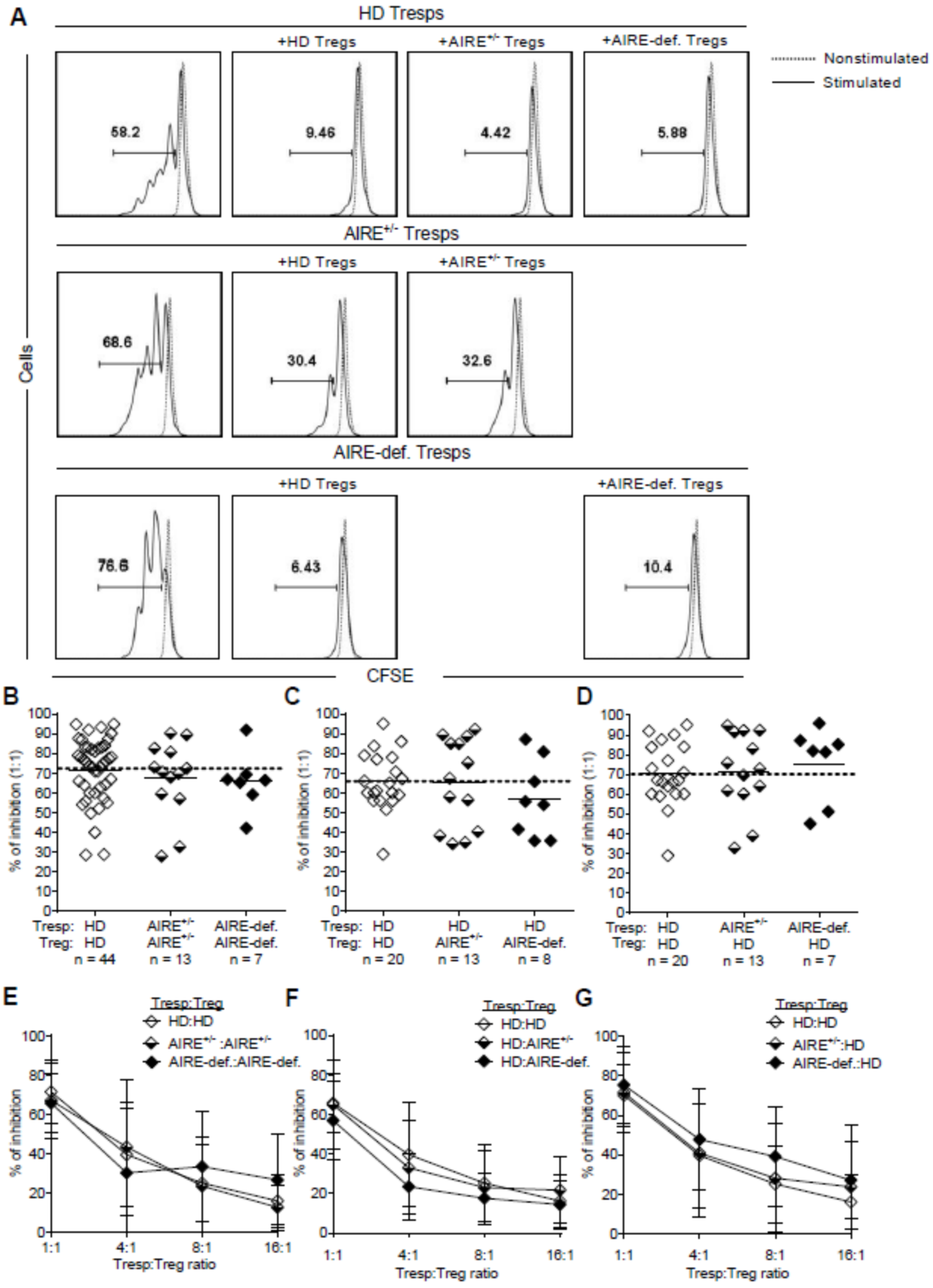
A
HD Tresps
+HD Tregs
+AIRE+/- Tregs
+AIRE-def. Tregs
Nonstimulated
Stimulated
58.2
9.46
4.42
5.88
AIRE+/- Tresps
+HD Tregs
+AIRE+/- Tregs
68.6
30.4
32.6
AIRE-def. Tresps
+HD Tregs
+AIRE-def. Tregs
76.6
6.43
10.4
Cells
CFSE
B
C
D
% of inhibition (1:1)
Tresp: HD AIRE+/- AIRE-def.
Treg: HD AIRE+/- AIRE-def.
n = 44
n = 13
n = 7
Tresp: HD HD HD
Treg: HD AIRE+/- AIRE-def.
n = 20
n = 13
n = 8
Tresp: HD AIRE+/- AIRE-def.
Treg: HD HD HD
n = 20
n = 13
n = 7
E
F
G
Tresp:Treg
HD:HD
AIRE+/- :AIRE+/-
AIRE-def.:AIRE-def.
HD:AIRE+/-
HD:AIRE-def.
AIRE+/-:HD
AIRE-def.:HD
% of inhibition
1:1
4:1
8:1
16:1
Tresp:Treg ratio

Fig. S13, related to Fig. 6. T_{regs} from both AIRE heterozygotes and AIRE-deficient patients have normal in vitro suppressive function. (A) Representative histograms of Treg mediated suppression of autologous and heterologous CFSE-labeled T responders on day 3.5 from an $AIRE^{+/-}$ heterozygous subject ($AIRE^{+/-}$) and an AIRE-deficient patient (AIRE-def.) compared with those from a healthy donor (HD). Dashed line shows non-stimulated T responders. (B) Autologous suppressive ability of Tregs from HDs, $AIRE^{+/-}$ subjects and AIRE-def. patients. (C) and (D) display the heterologous suppressive capacity of mixed Treg/Tresp co-cultures. Each symbol represents an individual, solid lines show the mean and dashed line indicates the averaged mean value for HDs. (E) Autologous and (F, G) heterologous suppressive ability of Tregs from healthy donors, $AIRE^{+/-}$ heterozygotes, and AIRE-deficient patients at lower Treg/Tresp ratios.

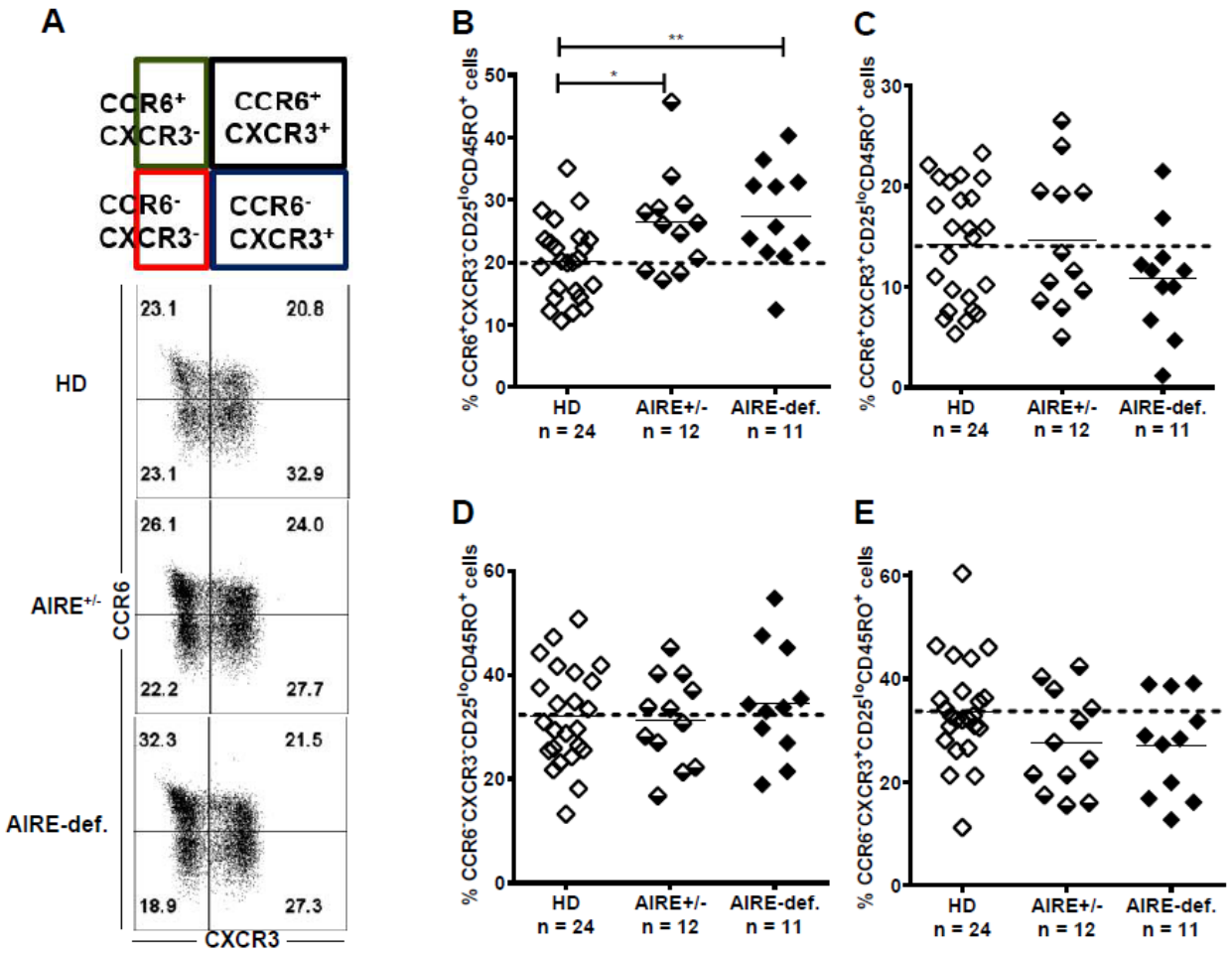

Fig. S14, related to Fig. 6. Elevated frequencies of CD3$^+$CD4$^+$CD45RO$^+$CCR6$^+$CXCR3$^-$ T cells in AIRE heterozygous individuals and AIRE-deficient patients. (A) Representative CXCR3 and CCR6 staining on CD3$^+$CD4$^+$CD8$^-$CD25$^-$CD45RO$^+$ T cells from a healthy donor (HD), an AIRE$^{+/-}$ heterozygous subject (AIRE$^{+/-}$) and an AIRE-deficient patient (AIRE-def.). Summarized frequencies of (B) CCR6$^+$CXCR3$^-$, (C) CCR6$^+$CXCR3$^+$, (D) CCR6$^-$CXCR3$^-$, and (E) CCR6$^-$CXCR3$^+$ T cells from each subject's group is shown. Each symbol represents an individual, solid lines show the mean and dashed line indicates the averaged mean value for HDs. Statistically significant differences are indicated.

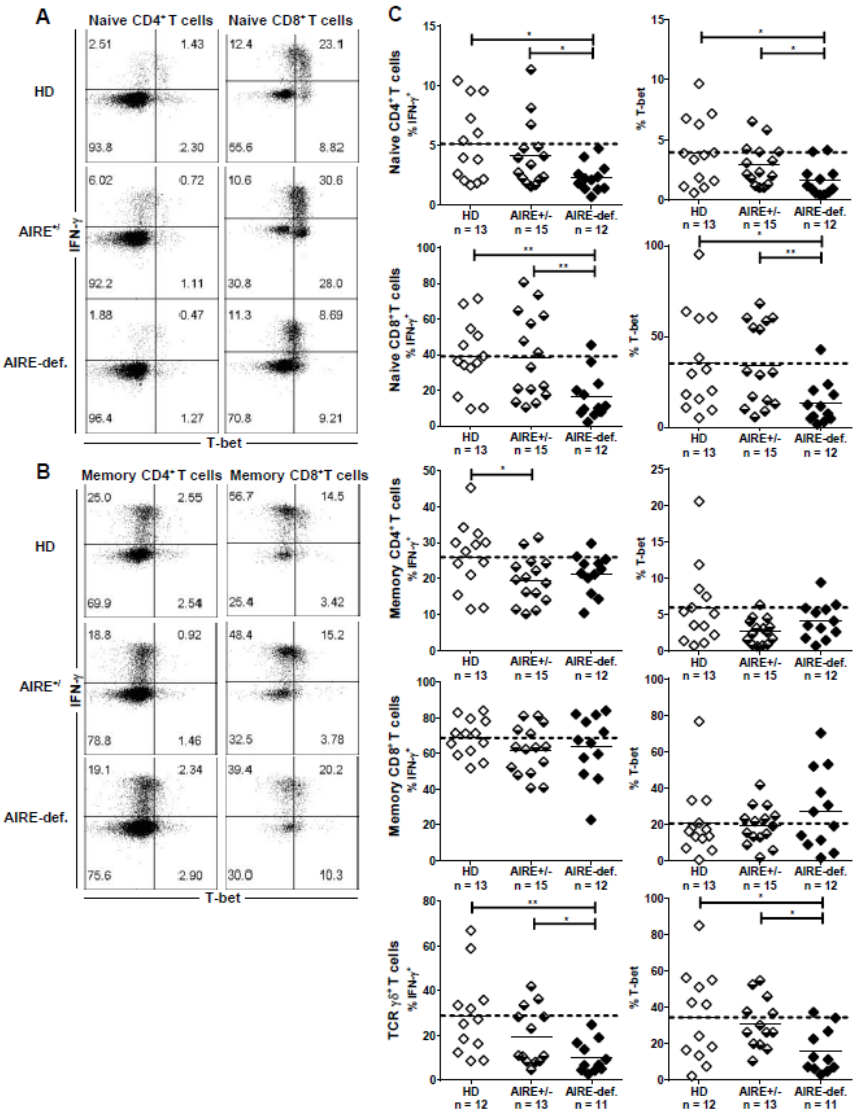

Fig. S15, related to Fig. 6. T cells from AIRE-deficient patients and AIRE heterozygous individuals exhibit reduced IFN-γ and T-bet expression during PMA-ionomycin activation. (A) Representative T-bet and IFN-γ staining on naïve $CD4^+$ (left) and naïve $CD8^+$ (right) T cells from a healthy donor (HD), an $AIRE^{+/-}$ heterozygous subject ($AIRE^{+/-}$) and an AIRE-deficient patient (AIRE-def.). (B) Representative T-bet and IFN-γ staining on memory $CD4^+$ (left) and memory $CD8^+$ (right) T cells from a HD, an $AIRE^{+/-}$ subject, and an AIRE-deficient patient. (C) Frequencies of IFN-γ^+ (left) and T-bet^+ (right) T cells in HDs, $AIRE^{+/-}$ subjects, and AIRE-deficient patients. Each symbol represents an individual, solid lines show the mean and dashed

line indicates the averaged mean value for HDs. Statistically significant differences are indicated.

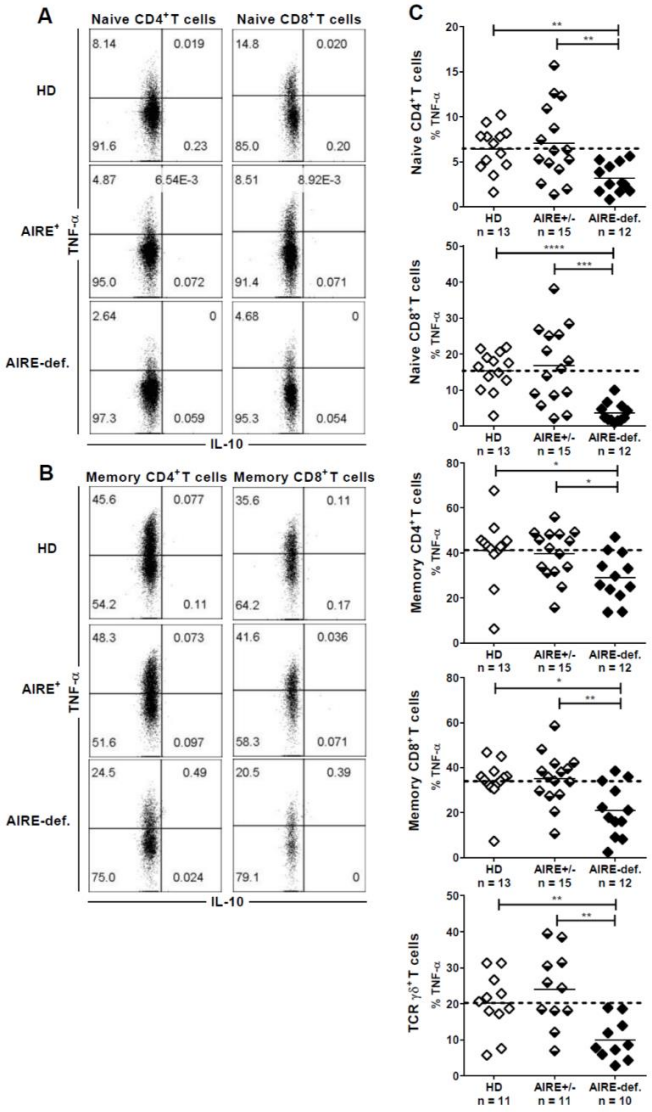

Fig. S16, related to Fig. 6. T cells from AIRE-deficient patients exhibit reduced TNF-α expression during PMA-ionomycin activation. (A) Representative IL-10 and TNF-α staining on naïve $CD4^+$ (left) and naïve $CD8^+$ (right) T cells from a healthy donor (HD), an $AIRE^{+/-}$ heterozygous subject ($AIRE^{+/-}$) and an AIRE-deficient patient (AIRE-def.). (B) Representative IL-10 and TNF-α staining on memory $CD4^+$ (left) and memory $CD8^+$ (right) T cells from a HD, an $AIRE^{+/-}$ subject, and an AIRE-deficient patient. (C) Frequencies of TNF-α^+ T cells in HDs, $AIRE^{+/-}$ subjects, and AIRE-deficient patients. Each symbol represents an individual, solid lines show

the mean and dashed line indicates the averaged mean value for HDs. Statistically significant differences are indicated.

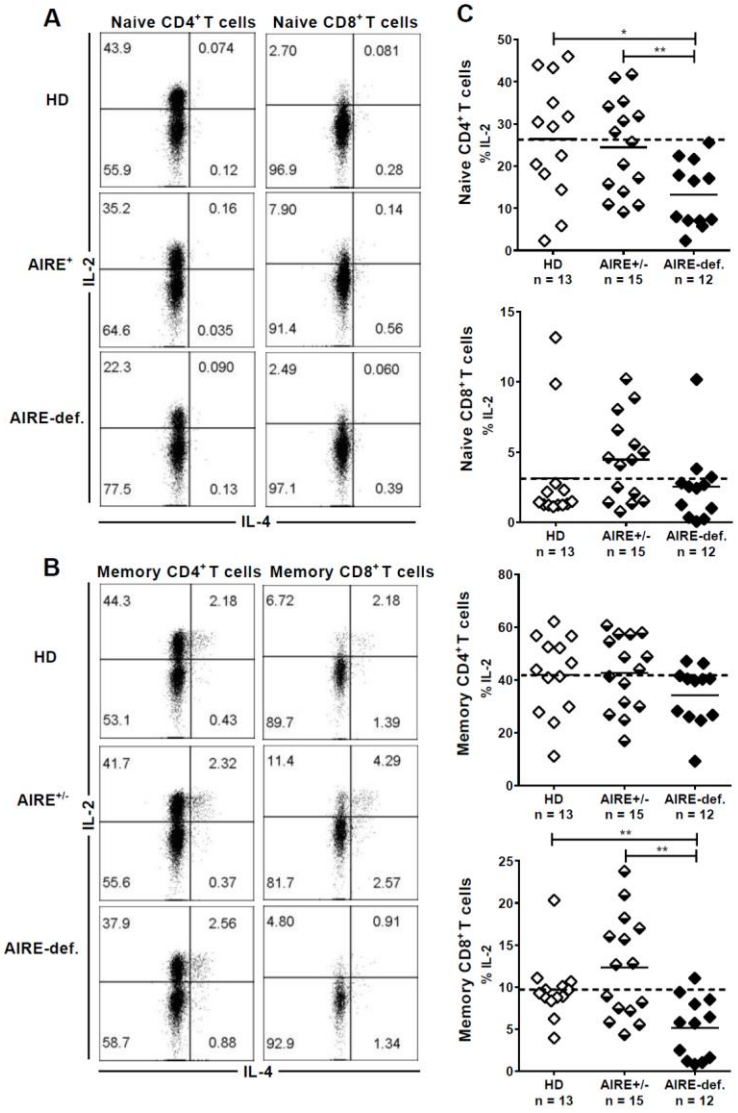

Fig. S17, related to Fig. 6. T cells from AIRE-deficient patients exhibit reduced IL-2 expression during PMA-ionomycin activation. (A) Representative IL-4 and IL-2 staining on naïve $CD4^+$ (left) and naïve $CD8^+$ (right) T cells from a healthy donor (HD), an AIRE+/- heterozygous subject ($AIRE^{+/-}$) and an AIRE-deficient patient (AIRE-def.). (B) Representative IL-4 and IL-2 staining on memory $CD4^+$ (left) and memory $CD8^+$ (right) T cells from a HD, an $AIRE^{+/-}$ subject, and an AIRE-deficient patient. (C) Frequencies of IL-2^+ T cells in HDs, $AIRE^{+/-}$ subjects, and AIRE-deficient patients. Each symbol represents an individual, solid lines show

the mean and dashed line indicates the averaged mean value for HDs. Statistically significant differences are indicated.

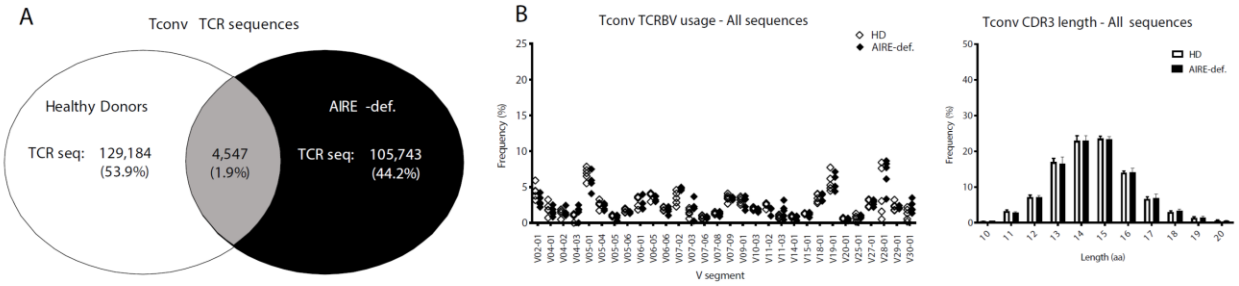

Fig. S18, related to Fig. 7. Similar global TCRBV segment gene usage in T_{conv} cells from HDs and AIRE-deficient patients. $CD4^{+}CD127^{+}$ Tconv cells were sorted by flow cytometry from healthy donor controls (HD, n=5) and AIRE-deficient patients (AIRE-def., n=5) and subjected to T cell receptor beta variable (TCRBV) sequencing. (A) Summary chart of Tconv CDR3 TCR sequences obtained from HD controls and AIRE-deficient patients. (B) TCRBV V gene segment usage and CDR3 length in Tconv from HDs and AIRE-deficient patients.

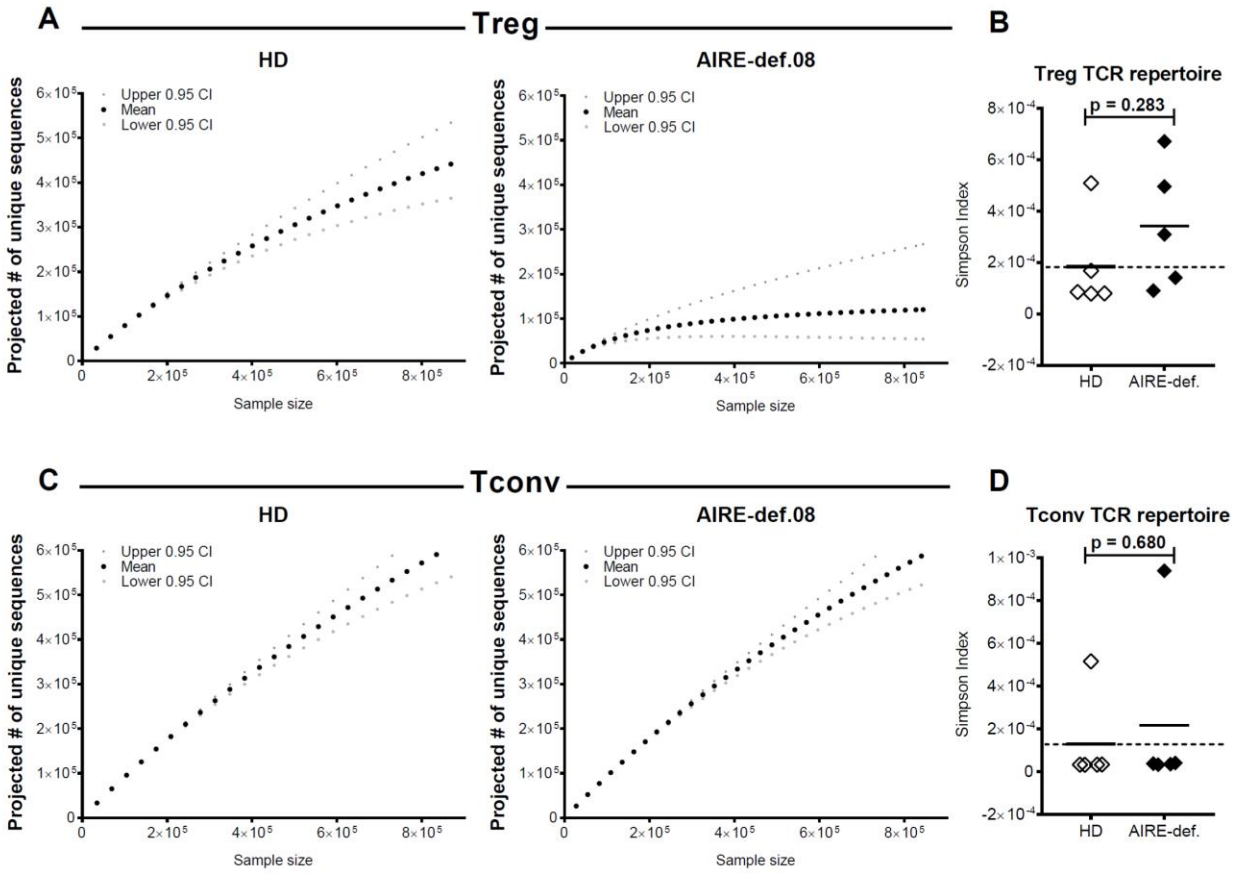

Fig. S19, related to Fig. 7. TCR diversity of T_{reg} and T_{conv} cells from HDs and AIRE-deficient patients. (A) Rarefaction analysis of the projected number of unique Treg TCR sequences in a representative healthy donor (HD) and an AIRE-deficient (AIRE-def.) patient. (B) Simpson Index analysis of Treg TCR diversity of 5 HDs and 5 AIRE-deficient patients. (C) Rarefaction analysis of the projected number of unique Tconv TCR sequences in a representative healthy donor (HD) and an AIRE-deficient patient. (D) Simpson Index analysis of Tconv TCR diversity of 5 HDs and 5 AIRE-deficient patients.

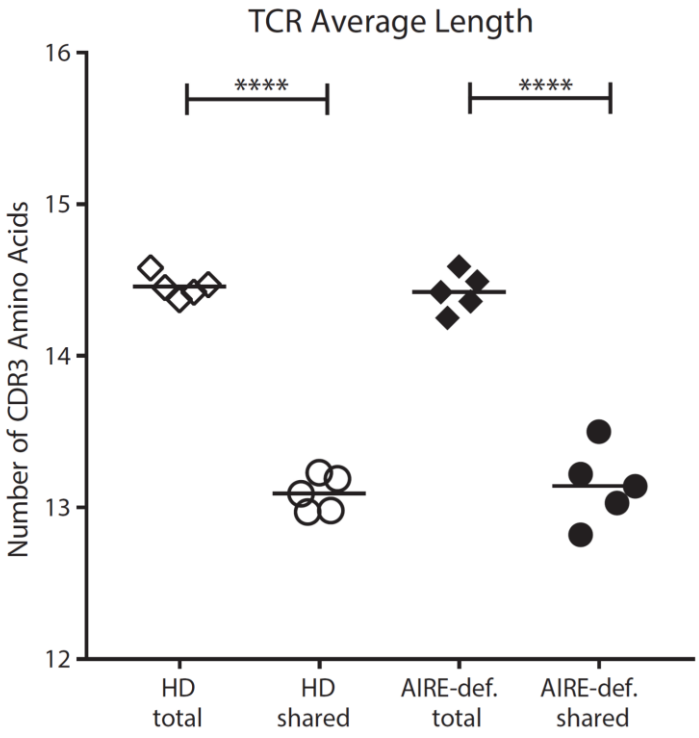

Fig. S20, related to Fig. 7. Reduced average CDR3 length in shared T_{reg} TCR sequences of HDs and AIRE-deficient patients.

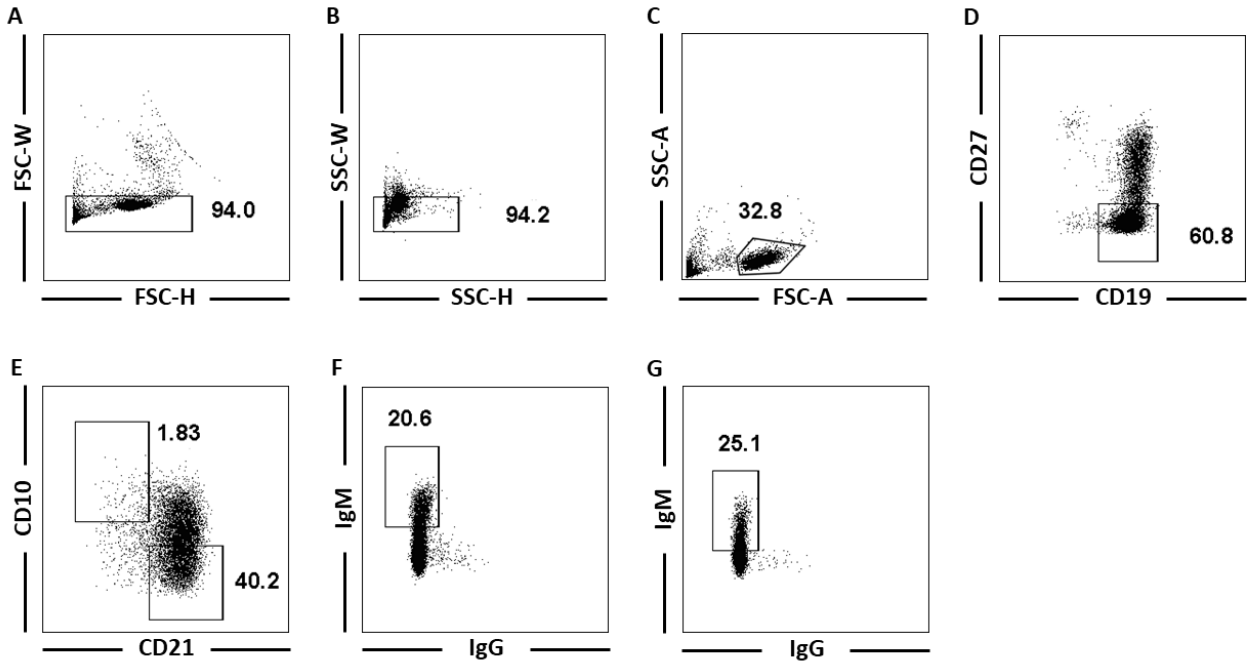

Fig. S21, related to Figs. 1 and 2. Example gating used for single B cell sort. The data corresponds with FACS sorted single $CD19^{+}CD27^{-}CD10^{+}IgM^{hi}CD21^{lo}$ new emigrant/transitional B cells and $CD19^{+}CD27^{-}CD10^{-}IgM^{+}CD21^{+}$ mature naïve B cells described in Fig 1 and 2. From left to right, doublet exclusion is invoked gating first on (A) FSC-H and FSC-W, followed by (B) SSC-H and SSC-W. Next, live lymphocytes are gated by (C) FSC-A and SSC-A, followed by gating on the naïve B cell subset (D) $CD19^{+}$ and $CD27^{-}$, followed by gating on (E) the $CD10^{+}CD21^{lo}$ (top left) and $CD10^{-}CD21^{+}$ (bottom right) subsets. The $CD10^{+}CD21^{lo}$ subset is subsequently gated on (F) the IgM^{hi} population to identify emigrant/transitional B cells, while the $CD10^{-}CD21^{+}$ subset is gated on (G) the IgM^{+} population to identify mature naïve B cells.

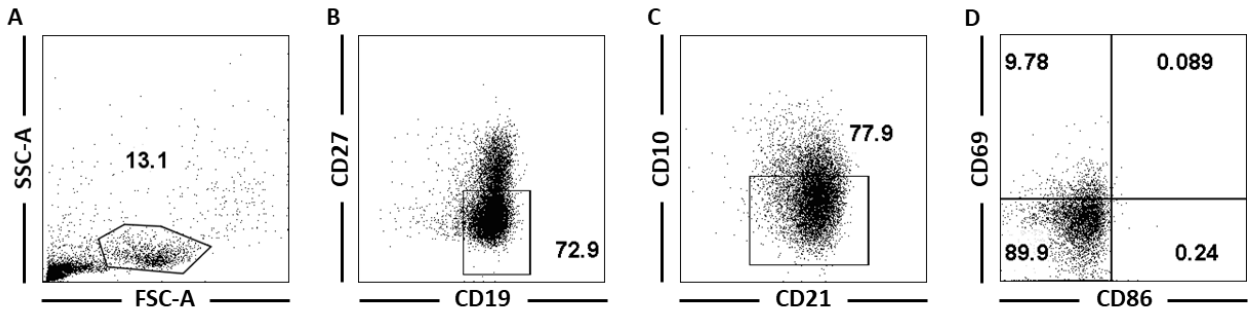

Fig. S22, related to Fig. 3A. Example gating used for B cell flow cytometry data. The data corresponds with CD19+CD27-CD21+CD10- mature naïve B cells shown in Fig. 3A. From left to right, gating first on (A) FSC-A and SSC-A, followed by gating on the naïve B cell subset (B) $CD19^{+}$ and $CD27^{-}$, followed by gating on the mature naïve B cell subset (C) $CD21^{+}$ and $CD10^{-}$. (D) CD86 and CD69 expression markers are thus displayed as seen in Fig. 3A.

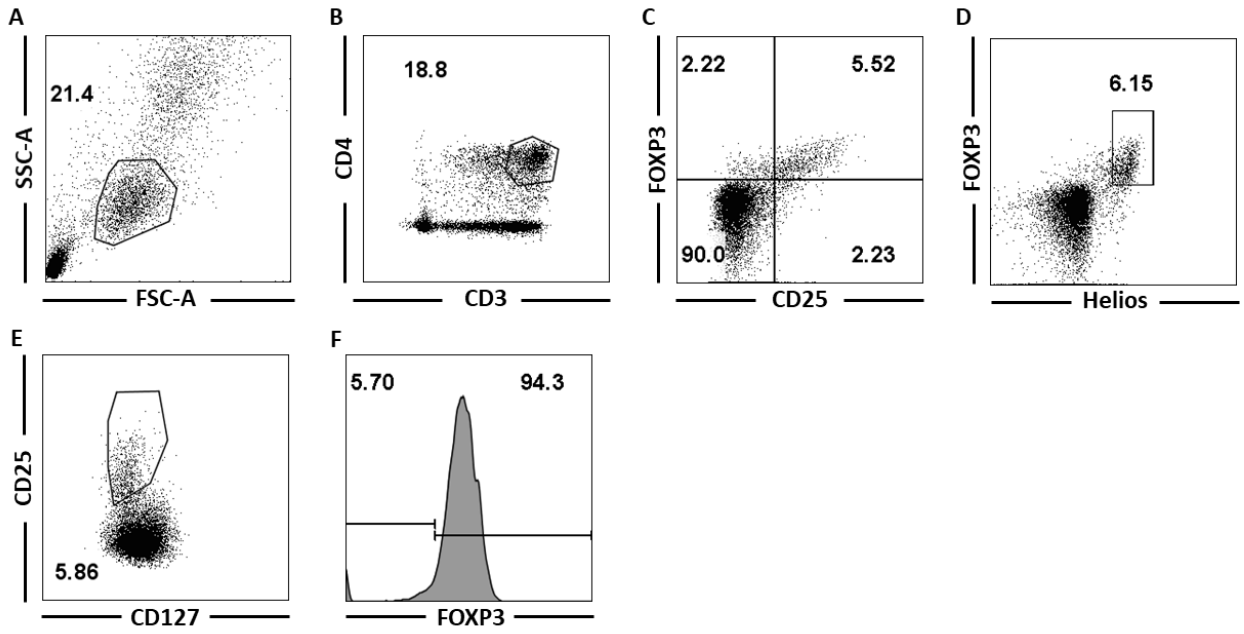

Fig. S23, related to Fig. 6, A to C. Example gating used for T_{reg} flow cytometry data. The data corresponds with $CD3^+CD4^+$ T cells shown in Fig. 6A. From left to right, gating first on (A) FSC-A and SSC-A, followed by gating on the $CD4^+$ T cell subset (B) $CD3^+$ and $CD4^+$, followed by gating on the (C) $CD25^+$ and $FOXP3^+$ subset or the (D) $Helios^+$ and $FOXP3^+$ subset displayed in Fig. 6A and summarized by Fig. 6C. $CD4^+$ T cells were also gated on (E) $CD127^{-/lo}$ and $CD25^+$ expression, followed by (F) $FOXP3^+$ expression and summarized in Fig. 6B.

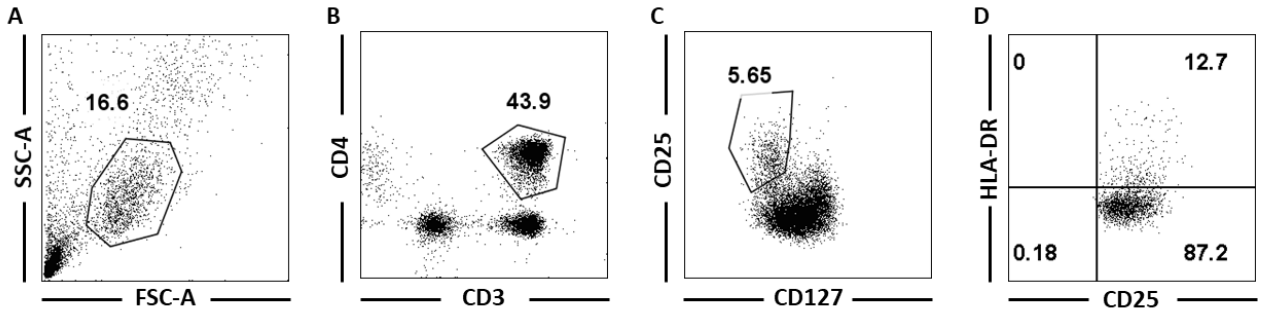

Fig. S24, related to Fig. 6, D and E. Example gating used for T_{reg} flow cytometry data. The data corresponds with $CD3^{+}CD4^{+}CD25^{+}CD127^{-/lo}$ T cells shown in Fig. 6D. From left to right, gating first on (A) FSC-A and SSC-A, followed by gating on the $CD4^{+}$ T cell subset (B) $CD3^{+}$ and $CD4^{+}$, followed by gating on the (C) $CD127^{-/lo}$ and $CD25^{+}$ subset, followed by gating on the (D) HLA-DR^{+} subset thus displayed as seen in Fig. 6D and summarized by Fig. 6E.

Table S1. AIRE mutations and deletions detected in the American APECED patient cohort.

Patient Code	Age in years at Sampling	Gender	Race / Ethnicity	Allele 1		Allele 2		Classic Triad			Other Clinical Manifestations
				DNA sequence	Protein sequence	DNA sequence	Protein sequence	CMC	Hypoparathyroidism	Adrenal Insufficiency	
AIRE01	2.75	F	White / Non-Hispanic	c.967_979del13	p.L232SfsX51	c.967_979del13	p.L232SfsX51	Yes	Yes	Yes	EH, KC, ID, Pneumonitis, SS, Urticaria, Vitiligo
AIRE02	12	M	White / Hispanic	c.1235delC	p.S412fsX373	c.1235delC	p.S412fsX373	Yes	No	Yes	ID, AIH
AIRE05	7	F	White / Non-Hispanic	c.967_979del13	p.L232SfsX51	c.769C>T	p.R257X	No	Yes	Yes	Alopecia, EH, ID, ND, Urticaria
AIRE07	8	F	White / Non-Hispanic	c.967_979del13	p.L232SfsX51	c.769C>T	p.R257X	Yes	Yes	No	EH, KC, ID, Urticaria
AIRE08	18	F	White / Hispanic	c.1094_1106del	p.L323fxX373	c.47C>T	p.T16M	Yes	Yes	Yes	AIH, EH, HT, ID, KC, ND, Pneumonitis, Urticaria
AIRE09	13	M	White / Non-Hispanic	c.967_979del13	p.L232SfsX51	c.967_979del13	p.L232SfsX51	Yes	Yes	Yes	EH, Urticaria
AIRE10	17	F	White / Non-Hispanic	c.967_979del13	p.L232SfsX51	c.967_979del13	p.L232SfsX51	Yes	Yes	Yes	Alopecia , EH, HT, KC, ND, OF, Urticaria, Vitiligo
AIRE11	17	F	White / Non-Hispanic	c.967_979del13	p.L232SfsX51	c.967_979del13	p.L232SfsX51	Yes	Yes	Yes	AIH, EH, Gastritis, HTN, ID, Pneumonitis, Urticaria, Vitiligo
AIRE13	10	F	White / Non-Hispanic	c.967_979del13	p.L232SfsX51	c.131A>C	p.Q44P	No	Yes	No	EH, HT, ID, Urticaria, Vitiligo
AIRE14	17	F	White / Non-Hispanic	c.967_979del13	p.L232SfsX51	c.769C>T	p.R257X	Yes	Yes	Yes	Gastritis, ID, Urticaria, Vitiligo
AIRE15	16	M	White / Non-Hispanic	c.242T>C	p.L81P	c.1265delC	p.P422fs	No	Yes	Yes	Alopecia, DM, EH, UE
AIRE16	20	M	White / Non-Hispanic	Homozygous 1735 base deletion spanning c.133-126_c.539-180del (spans exons 2-4)				No	Yes	Yes	ID, ND, UE, Vitiligo
AIRE17	18	F	White / Non-Hispanic	c.463+2T>C	p.P166L	c.463+2T>C	p.P166L	Yes	Yes	No	EH, ID, UE, Vitiligo
AIRE18	14	M	White / Non-Hispanic	c.463+2T>C	p.P166L	c.463+2T>C	p.P166L	Yes	Yes	No	EH, ID
AIRE19	10	M	White/Asian	c.769C>T	p.R257X	c.1364G>A	p.Trp455X	Yes	Yes	No	EH, ID, KC, UE, Vitiligo

Abbreviations: Autoimmune Hepatitis (AIH), Diabetes Mellitus (DM), Enamel Hypoplasia (EH), Hypertension (HTN), Hypothyrodism (HT), Intestinal Dysfunction (ID), Keratitis/Conjunctivitis (KC), Nail Dystrophy (ND), Ovarian Failure (OF), Testicular Failure (TF), Sjogren's-like Syndrome (SS).

Table S3. List of AIRE-dependent and AIRE-independent PTAs detected in protein microarray that were bound by recombinant antibodies cloned from new emigrant/transitional and mature naïve cells from HDs, AIRE$^{+/-}$ heterozygous individuals, and AIRE- and CD3-deficient patients.

Peripheral Tissue Antigen	AIRE-dependence	Ensembl ID	Gene Symbol	Aire_pos_TEC (mean counts)	Aire_ko_TEC (mean counts)	Fold Change	FDR (BH)
Actin	Yes	ENSMUSG00000031972	Acta1	187.9814784	86.71765399	0.461309565	0.048402107
	Yes	ENSMUSG00000035783	Acta2	1188.281402	379.1136564	0.319043667	1.14349E-27
	Yes	ENSMUSG00000068614	Actc1	292.0929595	15.12056631	0.051766281	5.35302E-13
Bone Morphogenetic Protein 4 (BMP4)	Yes	ENSMUSG00000021835	Bmp4	18.22565671	4.854039843	0.266330038	0.008217402
Collagen type VIII	Yes	ENSMUSG00000001506	Col1a1	3249.15691	104.3232101	0.032107778	1.93654E-34
	Yes	ENSMUSG00000029661	Col1a2	548.866171	208.0686501	0.379088129	7.27543E-12
Collagen type X	Yes	ENSMUSG00000026043	Col3a1	396.8858109	91.62966367	0.230871604	1.18745E-07
IFNα2	No						
IFNω	No						
IL-10	No						
IL-11	No						
IL-13	No						
IL-17A	Yes	ENSMUSG00000025929	Il17a	18.70810882	0	0	1.92493E-05
IL-17B	Yes	ENSMUSG00000024578	Il17b	293.577949	1.849249858	0.006299008	1.44028E-34
IL-17E	No						
IL-17F	Yes	ENSMUSG00000041872	Il17f	14.40367303	0.616416619	0.042795794	9.06349E-05
IL-20	No						
IL-21	Yes	ENSMUSG00000027718	Il21	82.45489795	11.48003643	0.139228072	9.39143E-09
IL-28A	No						
Insulin	Yes	ENSMUSG00000035804	Ins1	10.58168935	0	0	0.042407533
	Yes	ENSMUSG00000000215	Ins2	472.2060745	0	0	1.68588E-35
Kallikrein related peptidase 5 (KLK5)	Yes	ENSMUSG00000074155	Klk5	689.5042318	54.03017816	0.078360909	2.8511E-28
Macrophage-derived chemokine (MDC/CCL22)	Yes	ENSMUSG00000031779	Ccl22	8146.868785	2049.253109	0.25153874	4.80437E-51
Matrix metallopeptidase 3 (MMP-3)	Yes	ENSMUSG00000043613	Mmp3	83.48431619	0.597093341	0.007152162	8.38834E-22
Threonyl-tRNA synthetase (PL-7)	No						
Thyroid peroxidase (TPO)	Yes	ENSMUSG00000020673	Tpo	108.8553596	0.616416619	0.005662713	9.44125E-26
TWEAK/TNFSF12	No						

Table S4. Dissociation constants of recombinant antibodies cloned from new emigrant/transitional and mature naïve cells from HDs, AIRE$^{+/-}$ heterozygous individuals, and AIRE- and CD3-deficient patients.

Antigen affinity (K_D): New emigrant/transitional B cells									
Subject	**Clone**	**Insulin**	**IL-17A**	**IL-17F**	**Fibrinogen**	**MDC/CCL22**	**TWEAK**	**IFN-α**	**IFN-ω**
neHD10	L107	-	>10μM	-	-	-	-	-	-
neHD28	K11	1-10μM	-	-	-	-	-	-	-
neHD28	K26	-	-	-	-	>100μM	-	-	-
neAIRE$^{+/-}$05M	K15	>10μM	-	-	-	-	-	-	-
neAIRE-def.01	K52	-	-	>100μM	-	-	-	-	-
neAIRE-def.01	K61	>100μM	>10μM	-	-	-	-	-	-
neAIRE-def.01	L72	-	-	>100μM	-	-	-	-	-
neCD3E-def.	K14	-	-	-	-	-	1-10 μM	-	-

Antigen affinity (K_D): Mature naive B cells									
Subject	**Clone**	**Insulin**	**IL-17A**	**IL-17F**	**Fibrinogen**	**MDC/CCL22**	**TWEAK**	**IFN-α**	**IFN-ω**
mnHD09	K06	-	1-10μM	-	-	-	-	-	-
mnHD10	L02	-	>10μM	-	-	-	-	-	-
mnHD28	K11	-	-	>100μM	-	-	-	-	-
mnAIRE$^{+/-}$05M	K70	-	-	-	-	-	<1μM	-	-
mnAIRE$^{+/-}$05M	K85	-	-	-	1-10μM	-	-	-	-
mnAIRE-def.01	K15	-	-	>100μM	-	-	-	-	-
mnAIRE-def.01	K45	-	-	-	-	-	>10μM	-	-
mnAIRE-def.01	K47	>10μM	>10μM	-	-	-	-	-	-
mnAIRE-def.01	L19	1-10 μM	-	-	-	-	<1nM	1-10 μM	<1μM
mnAIRE-def.02	K62	-	-	-	-	-	1-10 μM	-	-
mnAIRE-def.02	K84	1-10μM	-	-	-	-	-	-	-
mnAIRE-def.05	L134	>10μM	-	-	-	-	-	-	-
mnAIRE-def.07	K81	-	0.389μM	-	-	-	-	-	-
mnCD3D-def.	K87	-	-	-	-	-	1-10nM	-	-
mnCD3D-def.	L62	-	-	-	-	-	<1nM	-	-
mnCD3E-def.	K92	-	-	-	-	-	<1nM	-	-

Table S5. List of protein microarray antigens.

	Analyte	Manufacturer, Product #
1	APRIL	Peprotech, 310-10C
2	BAFF	Peprotech, 310-13
3	BDNF	Peprotech, 450-02
4	EGF	Peprotech, AF-100-15
5	EPO	Peprotech, 100-64
6	GCSF	Peprotech, 300-23
7	GM-CSF	Peprotech, 300-03
8	HGF	Peprotech, 100-39H
9	HGH	Peprotech, 100-40
10	IFN-beta	Peprotech, 300-02BC
11	IFN-gamma	Peprotech, 300-02
12	IFN-imega	Peprotech, 300-02J
13	IL-10	Peprotech, 200-10
14	IL-11	Peprotech, 200-11
15	IL-12p40	Peprotech, 200-12P40
16	IL-12p70	Peprotech, 200-12
17	IL-13	Peprotech, 200-13
18	IL-15	Peprotech, 200-15
19	IL-16	Peprotech, 200-16
20	IL-17A	Peprotech, 200-17
21	IL-17B	Peprotech, 200-28
22	IL-17D	Peprotech, 200-27
23	IL-17E	Peprotech, 200-24
24	IL-17F	Peprotech, 200-25
25	IL-1b	Peprotech, 200-01B
26	IL-2	Peprotech, 200-02
27	IL-20	Peprotech, 200-20
28	IL-21	Peprotech, 200-21
29	IL-22	Peprotech, 200-22
30	IL-23	Peprotech, 200-23
31	IL-27	Peprotech, 200-38
32	IL-3	Peprotech, 200-03
33	IL-4	Peprotech, 200-04
34	IL-5	Peprotech, 200-05
35	IL-6	Peprotech, 200-06
36	IL-7	Peprotech, 200-07
37	IL-8	Peprotech, 200-08M

38	IL-9	Peprotech, 200-09
39	M-CSF	Peprotech, 300-25
40	CCL2 (MCP1)	Peprotech, 300-04
41	NOG	Peprotech, 120-10C
42	OSM	Peprotech, 300-10
43	SCF	Peprotech, 300-07
44	TGFB1	Peprotech, 100-21
45	TGFB2	Peprotech, 100-35B
46	TGFB3	Peprotech, 100-36E
47	TNF-beta	Peprotech, 300-01B
48	TNF-alpha	Peprotech, 300-01A
49	TPO	Peprotech, 300-18
50	TSLP	Peprotech, 300-62
51	VEGF 121	Peprotech, 100-20A
52	VEGF 165	Peprotech, 100-20
53	sCD40 Ligand/TRAP	Peprotech, 310-02
54	IL-29 (IFN-L1)	Peprotech, 300-02L
55	IL-28A (IFN-L2)	Peprotech,300-02K
56	CCL1	Peprotech, 300-37
57	CCL24 (Eotaxin-2)	Peprotech, 300-33
58	CXCL16	Peprotech, 300-55
59	CXCL13 (BCA-1/BLC)	Peprotech, 300-47
60	CCL3	Peprotech, 300-08
61	CCL5	Peprotech, 300-06
62	SPARC	Peprotech, 120-36
63	TARC	Peprotech, 300-30
64	ANG2	Peprotech, 130-07
65	EGFR	Peprotech, 100-15R
66	MDC	Peprotech, 300-36A
67	MIP3	Peprotech, 300-29
68	MIF	Peprotech, 300-69
69	MMP-3	Peprotech, 420-03
70	TWEAK	Peprotech, 310-06
71	BMP4	Peprotech, 120-05
72	IL-17A	R&D, 317-ILB-050
73	CXCL4	R&D, 795-P4-025/CF
74	IL-18	R&D, 9124-IL-050/CF
75	IL-26 monomer	R&D, 1375-IL-025/C
76	PDGFR-A	R&D, 322-PR-050/CF

77	CX3CL1	R&D, 365-FR-025/CF
78	HMGB1	R&D, 1690-HMB-050
79	CTGF	R&D, 9190-CC-050
80	TGFB RIII	R&D, 242-R3-100/CF
81	TNC	R&D, 3358-TC-050
82	sTNF RI/TNFRSF1A	R&D, 636-R1-025/CF
83	IFN-alpha2a	Prospec, CYT-204
84	TNF RII	Prospec, CYT-769
85	VEGF	Prospec, CYT-260
86	VEGFR2	Prospec, PKA-242
87	MMP-7	Prospec, ENZ-867
88	ISG15	Prospec, PRO-611
89	Fibrinogen 1	Prospec, PRO-2210
90	NPM1 (B23)	Prospec, PRO-1120
91	RPP30	Prospec, ENZ-040
92	FBL	Prospec, ENZ-566
93	KLK5	Prospec, ENZ-630
94	SAE1	Prospec, ENZ-534
95	DSG1	Abnova, H00001828-P01
96	DSG4	Abnova, H00147409-Q01
97	U1-snRNP 68	Diarect, A13001
98	U1-snRNP A	Diarect, A13101
99	U1-snRNP C	Diarect, A13201
100	La/SSB	Diarect, A12801
101	Ro 60/SS-A (bovine)	Diarect, A15501
102	Ro 60/SS-A (recombinant)	Diarect, A17401
103	Ro 52/SSA	Diarect, A12701
104	genomic double-stranded DNA	Sigma, D1626
105	plasmid double-stranded DNA	Diarect, A12301
106	Sm/RNP (SRC-3000)	Immunovision, SRC-3000
107	Smith (SMA-3000)	Immunovision, SMA-3000
108	U-snRNP B/B'	Diarect, A13301
109	Histone H1 (His-1001)	Immunovision, HIS-1001
110	Histone H2a & H4 (His-1002)	Immunovision, HIS-1002
111	Histone H2b (His-1003)	Immunovision, HIS-1003
112	Histone H3 (His-1004)	Immunovision, HIS-1004
113	Whole Histone (His-1000)	Immunovision, HIS-1000
114	Jo-1 (Histidyl-tRNA synthetase)	Diarect, A12901
115	Ku, p70/p80	Diarect, A17301

116	PCNA	Diarect, A15401
117	Ribosomal phosphoprotein P0	Diarect, A14101
118	Ribosomal phosphoprotein P1	Diarect, test lot 1193
119	Ribosomal phosphoprotein P2	Diarect, test lot 1179
120	CENP B	Diarect, A12501
121	CENP A	Diarect, A16901
122	PM/Scl 100	Diarect, A16001
123	PL-7	Diarect, A15601
124	PL-12	Diarect, A15701
125	Elastase	Arotec, ATE01
126	Azurocidin	The Binding Site, BH236.X
127	BPI	Arotec, ATB01-02
128	Mi-2	Diarect, A18101
129	TG	Diarect, A12201
130	TPO	Diarect, A12101
131	LC1	Diarect, A13701
132	LKM1	Diarect, A13501
133	b2GP I	Diarect, A14901
134	Actin	Molecular Probes, A12375
135	Scl-70, truncated	Diarect, A14501
136	GBM, undissociated	Diarect, A15901
137	GBM, dissociated	Diarect, A16801
138	Hsp70	Stressgen, NSP-555
139	Hsp90	Stressgen, SPP-770
140	Grp78	Stressgen, SPP-765
141	Hsp47	Stressgen, NSP-535
142	Hsp25	Stressgen, NSP-510
143	Hsp60	Stressgen, NSP-540
144	Scl-70, full-length	Diarect, A12401
145	MMP-9	Arotec, ATM03-02
146	NGAL	Arotec, ATN01-02
147	Intrinsic Factor	Diarect, A16701
148	Tissue Transglutaminase	Diarect, A15200
149	PM/Scl 75	Diarect, test lot 1137/2
150	Annexin V	Sigma, A9460
151	MPO	Diarect, 18501
152	PR3	Diarect, 18601
153	SRP54	Diarect, A18401
154	C1q	Biodesign, A90150H

155	LAMP-2	Diarect, test lot 99B06
156	M2 Antigen	Diarect, A18001
157	BCOADC-E2	Diarect, test lot 1201/2
158	PDC-E2	Diarect, test lot 359/1
159	gp210	Diarect, A19001
160	Sp 100	Diarect, A18901
161	Annexin V	Diarect, 19101
162	BPI	Diarect, Test lot 1352
163	Nup62	Diarect, 19401
164	SmD1	Diarect, 11801
165	SmD2	Diarect, 11901
166	SmD3	Diarect, 12001
167	SmD	Diarect, 11701
168	MDA5	Diarect, 30001
169	B2-Glycoprotein I	Surmodics, A14900
170	b2GP I non-recom. Human	Surmodics, A11300
171	b2GP I non-recom. Bovine	Surmodics, A11401
172	Gliadin	Diarect, 19501
173	GP2	Diarect, 19601
174	EJ (Glycycl-tRNA synthetase)	Diarect, 11101
175	TIF1-gamma	Diarect, 11001
176	Nucleolin	Diarect, 19701
177	Parietal cell antigen	Arotec, ATP01-04
178	Cardiolipin	Sigma, C1649
179	Cardiolipin	Sigma, C0563
180	Aggrecan	Sigma, A1960
181	Aggrecan	Biolegend
182	Fibrinogen type I-S	Sigma, F8630
183	Fibrinogen type IV	Sigma, F4753
184	Fibrinogen type I	Sigma, F3879
185	Laminin	Sigma, L2020
186	single-stranded DNA	Sigma, D8661
187	Aldolase, type X	Sigma, A2714
188	Vimentin	Sigma, V4383
189	Bare bead 1	
190	Myosin	Sigma, M1636
191	Collagen type IV	Sigma, C5533
192	Collagen type VI	Sigma, C7521
193	Human HDL	Academy Bio-medical, 80P-HD101

194	MDA-modified human LDL	Academy Bio-medical, 20P-MD-L110
195	PDH	Sigma, P7032
196	ECL-CAM	USBiological, E0275
197	Insulin	Sigma, I0908
198	Lipoprotein lipase	Sigma, L9656
199	Proteoglycans	Sigma, P5864
200	EBV EA-D	Biodesign, R18740
201	EBV EA	Prospec Bio, EBV-272
202	EBV EBNA-1	Prospec Bio, EBV-276
203	EBV P18	Prospec Bio, EBV-273
204	Collagen I	MBL, JM-4796-10
205	Collagen V	Abcam, ab7537
206	POLR3H	Fitzgerald 80R-2507
207	Catalase	Sigma, C3556
208	Bare bead 2	
209	XRCC4	Abnova, H00007518-P01
210	LIG4	Abnova, H00003981-Q01
211	XLF (NHEJ1)	Abnova, H00079840-P01
212	Ku80 (XRCC5)	Abnova, H00007520-P01
213	DNA PKcs (PRKDC)	Abnova, H00005591-Q01
214	GSN	Abnova, H00002934-P01
215	LTF	Abcam, ab90354
216	Lysozyme	Sigma, L8402
217	Cathepsin G	Enzo, BML-SE283-0100
218	RPP25	TP303538 Origene 20ug
219	RPP14	TP760291 Origene 50ug
220	U11/U12 RNP	Origene, TP303746, 20ug
221	MORC3	TP310530 Origene 20 ug
222	PDGFR-B	BioVision, 7493-50, 1x50 ug
223	Enolase	Sigma, E0379
224	Heparan sulfate	Sigma, H7640
225	Oxidized human LDL	Academy Bio-Medical, 20P-OX-L110
226	Hepatitis B surface antigen	Meridian Life Sciences, R36100
227	Collagen type II	Sigma, C1188
228	Collagen type VIII	Sigma, C7774
229	Collagen type IX	Sigma, C3657
230	Collagen type X	Sigma, C4407

231	a-actinin	Sigma, A9776
232	ssDNA 30ug	Sigma, D8899
233	ssDNA 15ug	Sigma, D8899
234	ssDNA 5ug	Sigma, D8899
235	GST 10ug	Sigma, G8642
236	Bare bead 3	
237	Fibrinogen 10ug	Sigma, F3879
238	Myosin 10ug	Sigma, M7659
239	ssDNA 30ug in MES	Sigma, D8899
240	ssDNA 15ug in MES	Sigma, D8899
241	ssDNA 5ug in MES	Sigma, D8899
242	IgG from human serum D1	Sigma, I2511-10MG
243	IgG from human serum D2	
244	IgG from human serum D3	
245	ChromPure Human IgG, Fc fragment D1	Jackson, 009-000-008
246	ChromPure Human IgG, Fc fragment D2	
247	ChromPure Human IgG, Fc fragment D3	
248	human IgE D1	Thermo Fisher, DIA HE1-01
249	human IgE D2	
250	human IgE D3	
251	IgM from human serum D1	Sigma, I8260-1MG
252	IgM from human serum D2	
253	IgM from human serum D3	
254	IgA from human colostrum D1	Sigma, 2636-5MG
255	IgA from human colostrum D2	
256	IgA from human colostrum D3	
257	AffiniPure Goat Anti-Human IgG, F(ab')2 fragment specific D1	Jackson, 109-005-097
258	AffiniPure Goat Anti-Human IgG, F(ab')2 fragment specific D2	
259	AffiniPure Goat Anti-Human IgG, F(ab')2 fragment specific D3	
260	AffiniPure Fab Fragment Goat Anti-Human IgG (H+L) D1	Jackson, 109-007-003
261	AffiniPure Fab Fragment Goat Anti-Human IgG (H+L) D2	
262	AffiniPure Fab Fragment Goat Anti-Human IgG (H+L) D3	
263	AffiniPure Rabbit Anti-Human IgG (H+L) D1	Jackson, 309-005-082
264	AffiniPure Rabbit Anti-Human IgG (H+L) D2	
265	AffiniPure Rabbit Anti-Human IgG (H+L) D3	
266	AffiniPure Goat Anti-Human IgG, Fcγ Fragment Specific D1	Jackson, 109-005-098
267	AffiniPure Goat Anti-Human IgG, Fcγ Fragment Specific D2	
268	AffiniPure Goat Anti-Human IgG, Fcγ Fragment Specific D3	
269	AffiniPure Rabbit Anti-Human IgG + IgM (H+L) D1	Jackson, 309-005-107

270	AffiniPure Rabbit Anti-Human IgG + IgM (H+L) D2	
271	AffiniPure Rabbit Anti-Human IgG + IgM (H+L) D3	
272	Goat Anti-Human IgM, Mouse/Bovine/Horse SP ads-UNLB D1	Southern Biotech, 2023-01
273	Goat Anti-Human IgM, Mouse/Bovine/Horse SP ads-UNLB D2	
274	Goat Anti-Human IgM, Mouse/Bovine/Horse SP ads-UNLB D3	
275	AffiniPure Goat Anti-Human IgM, Fc5μ fragment specific D1	Jackson, 109-005-129
276	AffiniPure Goat Anti-Human IgM, Fc5μ fragment specific D2	
277	AffiniPure Goat Anti-Human IgM, Fc5μ fragment specific D3	

Materials and Methods

Analysis of recomninant antibodies on the antigen arrays

6 µg of each antigen and a three-point dilution series of various control mouse and anti-mouse antibodies (0.25, 1, 4 µg) were diluted in PBS and transferred to 96-well plates. Diluted antigens and control antibodies were coupled to $1x10^6$ carboxylated magnetic beads per ID (MagPlex-C, Luminex Corp.). For this step, beads were distributed into 96-well plates (Greiner BioOne), washed and re-suspended in phosphate buffer (0.1M NaH_2PO_4, pH 6.2) using a plate washer (Biotek). Bead surface was activated by adding 100 µl of phosphate buffer containing 0.5 mg of 1-ethyl-3(3-dimethylamino-propyl)carbodiimide (Pierce) and 0.5 mg N-hydroxysuccinimide (Pierce). After 20 min incubation on a shaker (Grant Bio), beads were washed and re-suspended in activation buffer (0.05M MES, pH 5.0). Diluted antigens and control antibodies were incubated with beads for 2 hours at RT. The beads were washed 3 times in 100 µL PBS-T, re-suspended in 60 µL storage buffer (Blocking reagent for ELISA, Roche) and stored in plates at 4°C overnight.

Immobilization of the antigens and control antibodies on the correct bead IDs were confirmed by analysis of the following commercially available mouse monoclonal antibodies: anti-La/SSB (Santa Cruz), anti-Ro52 (Santa Cruz), anti-His6 tag (Invitrogen), anti-Scl70 and anti-SSB (Immunovision), anti-IL1, anti-IL2, anti-IL4, anti-IL5, anti-IL6, anti-IL10, anti-IL13, anti-IL17A, anti-CCL2, anti-IFN-β and anti-IFN-γ (eBiosciences), and anti-GM-CSF (Biolegend), all analyzed at 1 µg/mL (data not shown). In addition, dilution series (1:50 to 1:300) of various autoimmune disease state human plasma for ds-DNA, Scl-70, SSA, SSB, cardiolipin, whole histones and RNP (Immunovision), as well as normal human sera (Immunovision) were used to validate the content of the array (data not shown). Following this, two antibody pools (one for the mature naïve and one for new emigrant/transitional B cell fraction) were prepared for each of the nine donors (two HD, three $AIRE^{+/-}$ subjects and four AIRE-deficient patients). The 18 antibody pools

were analyzed with the bead array as a dilution series (1:62.5 to 1:1000) to choose the optimal sample dilution (data not shown).

Based on the optimized assay conditions, all individual antibody clones were diluted 1:65 in an assay buffer of 0.05% PBS-T supplemented with 3% (w/v) BSA (Sigma). The bead array was distributed into 384-well plates (Greiner BioOne) by transfering 5 µL bead array per well and 45 µL of the 1:65 diluted antibody clones were added into the 384-well plate. Samples were incubated for 90 min on a shaker (Grant Bio) at RT. The beads were washed with 3 × 60 µl PBS-T on a plate washer (EL406, Biotek), followed by addition of 50 µl of R-PE conjugated AffiniPure F(ab')$_2$ fragment goat anti-human IgG, Fcγ fragment specific (Jackson), diluted 1:500 in a buffer consisting of 3% BSA in 0.05% PBS-T. After incubation with the secondary antibody for 45 min, plates were washed with 3 × 60 µL PBS-T and re-suspended in 60 µL PBS-T, then analyzed on a FlexMap3D instrument (Luminex Corp.). At least 100 events per bead ID were counted and binding events were displayed as median fluorescence intensity (MFI). Data were analyzed using R. Heatmaps were rendered using the pheatmap package following log2-transformation and scaling, where first a scaling factor matrix was built by calculating the median MFI vector over all antigens per sample, followed by dividing MFI values for each antigen by this scaling factor matrix.

Plasmon resonance analysis

Binding studies were performed at 25°C using a Biacore T100 optical biosensor (GE HealthCare, Biacore, Piscataway, NJ). The antigens were immobilized on a CM5 research-grade sensor chip using amine coupling and IL-17A protein (R&D Systems cat. number: 7955-IL-025/CF) at 20 µg/ml solution in 10 mM acetate buffer pH 4.5; IL-17F protein (PeproTech cat.number: 200-25) at 20 µg/ml solution in 10 mM acetate buffer pH 4.5; Insulin

(MilliporeSigma cat.number: I2767) at 20 µg/ml solution in 10 mM acetate buffer pH 4.75, Bovine Serum Albumin (MilliporeSigma cat.number: A9647) at 20 µg/ml solution in 10 mM acetate buffer pH 4.5; TWEAK (PeproTech cat.number: 310-06-25) 20µg/ml in 10 mM acetate buffer pH 5.5, Fibrinogen (MilliporeSigma cat.number: F3879) 20µg/ml in 10 mM acetate buffer pH 4.0, Collagen (MilliporeSigma cat.number: C7774) 100µg/ml in 10 mM acetate buffer pH 4.0, IFN-ω (Fisher Scientific cat.number: BMS304) 10µg/ml in 10 mM acetate buffer pH 4.5, IFN-α2 (BioLegend cat.number: 592704) 20µg/ml in 10 mM acetate buffer pH 4.5; MDC/CCL22 (PeproTech cat.number: 300-36A) at 20 µg/ml solution in 10 mM acetate buffer pH 5.5; KLK5 (R&D Systems cat. number: 1108-SE-010) at 13 µg/ml solution in 10 mM acetate buffer pH 5.0. High density chips were used that contained ~5-6 kRUs of IL-17A, 10.6 kRUs of IL-17F, 1.2-1.5 kRUs of Insulin, 7-9 kRUs of BSA., 10 kRUs for TWEAK, 10 kRUs for Firbrinogen, 6.8 kRUs for Collagen, 6.6 kRUs for IFN-ω, 2.1 kRUs for IFN-α2, 6.0 kRUs of MDC/CCL22, 3.9 kRUs of KLK5. Antibodies were injected from three fold dilution series starting with either 3 or 1 µM stock using a single-cycle approach [64]. The surfaces were regenerated by 30 second injections of 3M $MgCl_2$. The binding responses were double-referenced against the non-specific binding to dextran alone and injections of buffer alone. Binding affinity was determined by either fitting the amplitudes observed during the steady-state phase, or kinetics of the binding reaction, to a simple 1:1 binding model using BioEvaluation software (GE HealthCare, Biacore, Piscataway, NJ).